International Civil Aviation Organization

FOURTEENTH MEETING OF THE COMMUNICATIONS/NAVIGATION/SURVEILLANCE AND METEOROLOGY SUB-GROUP OF APANPIRG (CNS/MET SG/14)

Jakarta, Indonesia, 19 – 22 July 2010

Agenda Item 5: Navigation

3) discuss issues related to implementation of GNSS and review developments that have taken place in the Region

RESOLUTION FOR IONOSPHERE ISSUES IN IMPLEMENTING GNSS

(Presented by Japan)

SUMMARY

This Working Paper highlights the effects of the ionosphere on GNSS and suggests desirable actions to implement GNSS for aviation in a more advanced manner in APAC region. The effects of low latitude ionosphere on GNSS are reviewed. Ionosphere Field monitor is introduced as possible mitigation of the ionospheric impact on GBAS. Toward the next solar maximum, importance of coordinated ionosphere data collection in APAC region is emphasized. An example of local-area ionosphere observation system operated by Electronic Navigation Research Institute (ENRI) in the southwest part of Japan is introduced. Finally, workshops on the ionosphere and GNSS are suggested to enhance understandings of this topic in the APAC region.

This paper relates to:

Strategic Objective:
A. Safety D. Efficiency

Global Plan Initiative:
GPI – 5 RNAV and RNP (Performance Based Navigation)
GPI – 21 Navigation

1. Introduction/Background

1.1 The Navigation Strategy and the Performance-Based Navigation Roadmap for the Asia/Pacific Regions have prescribed to implement GNSS with augmentation as required for APV and precision approach operations where operationally required and economically beneficial and to implement the use of APV operations in accordance with ICAO's requirement. Following this strategy, Japan seeks implementation of SBAS and GBAS for APV and precision approach operations.

1.2 In the last APANPIRG/20 meeting held in Bangkok in September 2009, it was understood that the ionosphere is a significant issue in utilizing GNSS for aviation. It was also concluded that States are urged to cooperate with each other to collect data and characterize ionosphere model in the APAC region that will lead to smooth introduction of GNSS in the ASIA/PAC region and provide the name and contact details of the Focal Point of Contact to ICAO Regional Office for coordinating collection and exchange of ionosphere data with the ultimate objective of establishing a standard ionosphere model for the region.

2. Discussion

2.1 The ionospheric plasma between GNSS satellites and receivers affects radio wave propagation. Plasma in the ionosphere changes the refraction index and thereby the propagation velocity from the velocity of light in the vacuum. The total number of 10^{16} electrons per square meter is expressed as 1 TECU. The group velocity of the radio wave is delayed by 0.16, 0.27 and 0.29 m per TECU at GPS L1 (1.57542 GHz), L2 (1.22760 GHz) and L5 (1.17645 GHz) frequencies, respectively. The ionospheric plasma density and the delay increase with the solar activity. The vertical TEC can be as large as 100 TECU during the solar maximum. This corresponds to delays of 16, 27, and 29 m at L1, L2, and L5 frequencies, respectively. Smoothing filter utilizing carrier-phase measurement to reduce noise in pseudo-range measurement, which is used in SBAS and GBAS, enhances the error, because the pseudo-range and carrier-phase measurements have opposite polarities of responses to the ionospheric plasma. Position errors can be significantly larger than the values of range errors depending on satellite geometry. Ionospheric effects on GNSS for aviation have been documented in the ICAO NSP report (“Ionospheric Effects on GNSS Aviation Operations”, December 2006).

2.1.1 SBAS and GBAS are based on the differential GNSS technique where corrections to users are made based on observations at reference stations on the ground. If the ionospheric delay were homogeneous, the correction would be very accurate. However, the ionospheric delay is inhomogeneous in reality. Unless the ionospheric delay distribution is perfectly modelled, the difference in delays along the GNSS signal paths of the user and the reference stations results in correction error. Figure 1 shows such a basic idea. In GBAS and SBAS, systems must be designed so that the user is protected against such errors.

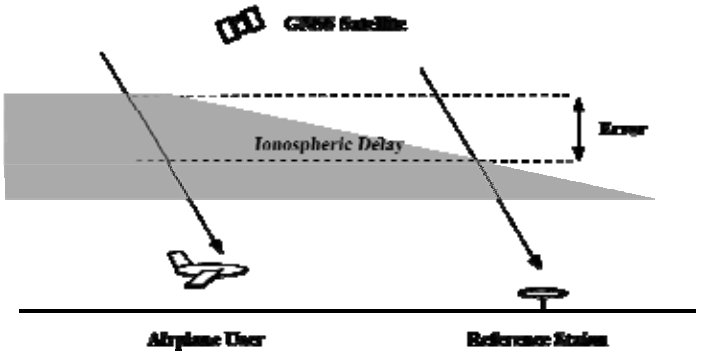

Figure 1. Inhomogeneous ionosphere and differential GNSS.

2.1.2 One of the ionospheric phenomena which accompany significant inhomogeneity (or gradient) in the ionospheric delay is so-called Storm Enhanced Density (SED) associated with a severe magnetic storm. It is observed in the mid to high magnetic latitude regions. This is relatively well studied in GBAS and SBAS. In the magnetic low latitude regions where the many of States in the APAC region is located, there are characteristic ionosphereic phenomena that accompany large ionospheric gradient. One is so-called equatorial ionization anomaly (EIA) that is a pair of belts where ionospheric plasma density is high and having peaks around ±15º in magnetic latitude (Figure 2a). EIA always exists, but the location and intensity significantly change in time to time. Another one is so called Equatorial Plasma Bubble (EPB) that is a sharp depletion of the ionospheric plasma. At the

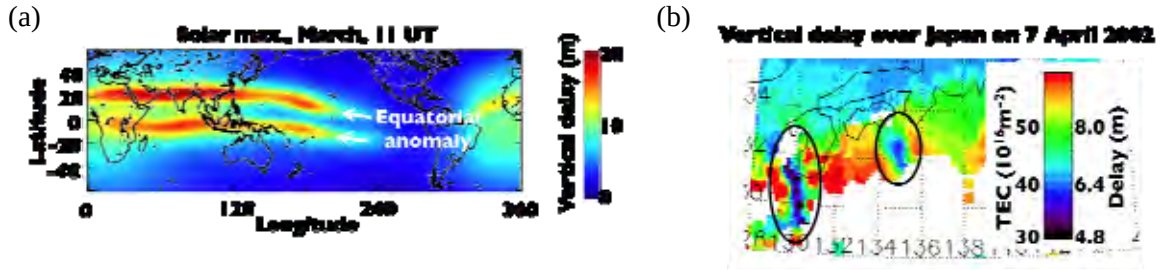

Figure 2. (a) Example of global ionospheric delay distribution derived from an empirical model (NeQuick). (b) Ionospheric delay distribution with the presence of two EPBs observed over Japan.

edges of EPB, the ionospheric gradient can be as large as that of SED. Figure 2b shows the ionospheric delay measured in Japan with the presence of two EPBs. It occurs frequently in the evening during the solar maximum and most of EPBs occur in a magnetic quiet condition. More information on EPB can be found in Attachment 1 of this Working Paper. EPB also accompany the strong scintillation in GNSS signals that may degrade the ranging accuracy, and may result in signal lock-off.

2.1.3 Electronic Navigation Research Institute (ENRI) is developing its original prototype of GBAS, which satisfies the SARPs requirements for CAT-I operation (vertical alert limit of 10 m) under the ionospheric environment in Japan taking both SED and EPB into account. ENRI has investigated the ionospheric condition over Japan, which is located from mid to low latitudes, and developed its own ionosphere threat model applicable to the ionosphere over Japan. Based on the investigation, it has been concluded that Ionosphere Field Monitor (IFM) located on the ground near DH to detect ionospheric gradient (Figure 3) is a solution to mitigate the potential risk of the ionosphere. With the IFM that is located closer to the approaching airplane than the reference stations, the maximum possible range errors induced by ionospheric gradient can be reduced. In many of States in this region located in lower magnetic latitudes than Japan, the ionospheric condition would be more severe. Therefore, ionospheric condition must be investigated carefully.

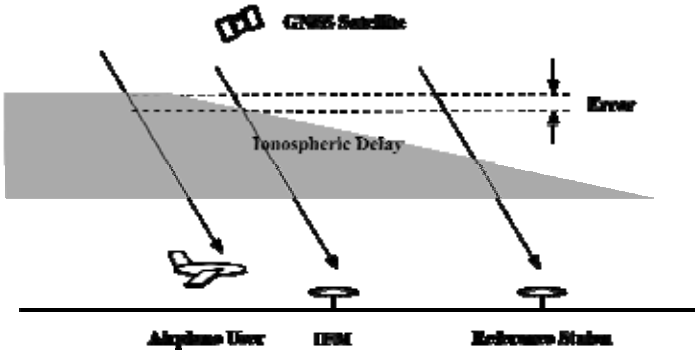

Figure 3. Effect of IFM to reduce ionosphere induced error in GBAS.

2.2 Evaluating and specifying the ionospheric threat is the responsibility of each State. Appropriately modelling the ionosphere based on good knowledge on the ionosphere is the key issue. However, it has not been established well mainly due to lack of enough data specifically needed by aviation applications. Toward the coming solar maximum expected around 2013, it is an urgent task to collect data in the APAC region.

2.2.1 The most important but lacking data is the ionospheric gradient measurement. In the case of EPB, the ionospheric delay can change from that of background to inside in a few tens kilometres. Therefore, it is necessary to measure the ionospheric delay at multiple receivers separated by several to ten kilometres. To understand the background conditions and EIA variations, wide-area observations of the ionospheric delay by GNSS receiver network is necessary. Scintillation measurement is also important to understand the relationship between EPB and scintillation. EPB drift velocity can be estimated by scintillation measurements by closely spaced (by a few hundred metres) receivers. EPB velocity measurement data is useful to build a model of EPB motion for future EPB propagation prediction. More detailed description on scintillation measurement by closely spaced receivers and EPB velocity estimation can be found in Attachment 2.

2.2.2 For delay measurement, local or wide-area, dual-frequency GNSS receivers with land survey quality can be used. For local-area observation, three or more receivers separated by several to ten kilometres which should not be aligned in a straight line. For wide-area delay observation, a network of receivers separated by a hundred kilometres or less is prefereable. For scintillation measurement, high sampling rate GNSS receivers dedicated for scintillation measurements should be used. Three or more scintillation receivers should be installed with distances of a few hundred metres and not aligned in a straight line.

2.2.3 ENRI is operating a local area gradient/scintillation observation system in Ishigaki Island (24.3ºN, 124.2ºE) in the southwest part of Japan. In Ishigaki, four stations equipped with a dual frequency (L1 and L2) GPS receiver and a scintillation receiver. The distances are from 400 m to 1 km. The distribution is rather optimized for scintillation measurements. However, similar system can be deployed for gradient measurement with longer distances. Detailed description of the Ishigaki system can be found in Attachment 3.

2.2.4 Wide-area measurements can be conducted collaborating with other organizations, such as International GNSS Service (IGS) or land survey networks in each State. Local gradient measurements could also be conducted by adding GNSS receivers near the existing stations. To start working on this issue quickly by utilizing existing facilities, to complement each other, and to avoid duplication, cooperation/coordination with other organizations or activities should be pursued. Other organizations or activities may include Interoperability Working Group (IWG) for SBAS or International GBAS Working Group (I-GWG).

3. Action by the Meeting

3.1 To develop a reliable ionosphere model in APAC region, data should be collected as much as possible. Since the next solar maximum is coming closer in a few years, it is important to share/exchange data to increase the total amount of data. For this purpose, a common way of data analysis and a common data format should be desirable. They should be further discussed in the frame of CNS/MET subgroup or between the States that are interested in ionosphere data collection.

3.2 To enhance understandings of contracting States on the ionosphere and GNSS, ICAO APAC Regional Office should organize workshops on the ionosphere and GNSS. For this purpose, a voluntary group for planning the workshop should be formed by utilizing the Focal Point of Contact. The planning should include preparing agenda and suggesting lecturers and invited speakers.

3.3 The meeting is invited to:

a) note the contents of the Working Paper;

b) encourage contracting States in APAC region to;

- collect data in each territory and share it with other contracting States toward the expected next solar maximum around 2013

c) task APAC Regional Office to;

- organize workshops to enhance understandings contracting States on the ionosphere and GNSS
- form a voluntary group for planning the workshop to prepare agenda and suggest lectures and invited speakers
- take necessary actions to coordinate ionosphere data collection with other organization

– – – – – – – – – – – –

ATTACHMENT 1

S. Saito, T. Yoshihara, and N. Fujii, Study of Effects of the Plasma Bubble on GBAS by a Three-Dimensional Ionospheric Delay Model, Proceedings of ION GNSS 2009.

Study of Effects of the Plasma Bubble on GBAS by a Three-Dimensional Ionospheric Delay Model

Susumu Saito, Takayuki Yoshihara, and Naoki Fujii, *Electronic Navigation Research Institute, Japan*

BIOGRAPHY

Susumu Saito received his B. S. degree in Physics at Nagoya University in 1995. He received his M. S. and Ph.D degrees in Ionospheric Physics in 1997 and 2001. From 2000 to 2008, he studied Ionospheric Physics from high to low latitudes at University of Tromsø in Norway, Kyoto University, and National Institute of Information and Communications Technology in Japan. From 2008, he joined Independent Administrative Institute, Electronic Navigation Research Institute (ENRI) in Japan. He is involved as a senior researcher in a project to develop a Ground-Based Augmentation Systems (GBAS) suitable for Japan. His research is focused on ionospheric effects unique to the low latitude ionosphere on GBAS.

Takayuki Yoshihara is a senior researcher at ENRI. He received his Ph.D. in GPS application for meteorology from Kyoto University, 2001. He is working in the field of atmospheric effects on GPS satellite signals, including evaluation of their impacts on GBAS.

Naoki Fujii is a Principle Researcher of ENRI. He received B.S. degree and M.S. degree in physics from Kobe University. He was charged with development of the siting criteria of Instrument Landing System (ILS), Microwave Landing System (MLS), Aircraft Address Monitoring System (AAMS) using Multi-lateration method of Second Surveillance Radar (SSR) signal, and the GPS downward-looking occultation technique observed on aircraft. He is currently working in the field of the development and evaluation of GBAS for Global Navigation Satellite System (GNSS).

ABSTRACT

Spatial gradient of the ionospheric plasma density is one of the most serious error source of differential GPS systems. Since Japan is located at relatively low magnetic latitudes (from 41 down to 19 degrees magnetic latitude), effects of low latitude ionospheric phenomena, especially a plasma bubble which is a region of depleted plasma density must be taken into account with great care.

A 3-D ionospheric delay model which take into account the effect of the plasma bubble has been developed based on the NeQuick ionospheric/plasmaspheric plasma density model and on knowledge on the plasma bubble obtained in more than 30 years history of its study.

GBAS is simulated (without any monitors) with our ionospheric model to investigate the impact of the plasma bubble on GBAS. Simulations are conducted with various satellite geometry, various plasma bubble location, and different approach directions. The results show that a single plasma bubble can cause a positioning error in vertical more than 10 m and needs to be detected by ground or airborne monitors. It is found that the impact of the plasma bubble is more significant when it comes around the meridian of the reference station, and not significant when it is located far east or west of the reference station. This result can be obtained only with a 3-D model which takes the plasma bubble structure into account. However, plasma bubbles in the real world generally have complex shapes, and multiple plasma bubbles are often observed at the same time. Considering these facts, the impact of plasma bubbles at low elevations in the east or west should be evaluated more carefully with more complex-shaped plasma bubbles, for example, based on the observation by VHF backscatter radars or airglow imagers.

Our simulation code is designed so that various simulation parameters are flexibly chosen, monitors can be easily implemented, multiple plasma bubbles can be considered. Complex-shaped plasma bubbles will also be tested. Our model can be utilized not only for GBAS but also for SBAS or other applications.

Our model shows reasonable and promising performance in modeling the ionospheric delay with a plasma bubble. It is quite useful in studying effects of plasma bubbles on GBAS to implement it in low latitude region, although our model needs more improvements which are being in progress. We believe that this kind of simulating tools are very necessary to potential GBAS systems in low latitude regions.

1 INTRODUCTION

Spatial gradient of the ionospheric plasma density is one of the most serious error source of differential GPS systems. The storm enhanced density (SED) which is asso-

ciated with a severe magnetic storm has been considered to be the most important ionosphere-origin threat for the ground based augmentation system (GBAS). Since North America and Europe are located at relatively high magnetic latitudes (no lower than 30 degrees magnetic latitude) in mid-latitudes, effects of the low latitude ionospheric phenomena, such as equatorial anomaly development or plasma bubbles have not been considered seriously.

Since Japan is located at relatively low magnetic latitudes (from 41 down to 19 degrees magnetic latitude), however, effects of low latitude ionospheric phenomena, especially a plasma bubble which is the region of depleted plasma density must be taken into account with great care. It is characterized by sharp plasma density gradients at its edges and various scale plasma density irregularities that cause radio scintillation.

The sharp plasma density gradient could increase the differential error between a ground reference station and an airborne equipment and may threaten the integrity of the GBAS. Radio scintillation could degrade the ranging accuracy, and sometimes cause receiver lock-off, which may also reduce the availability of the GBAS.

In contrast to the SED which is a rare phenomenon associated with a severe magnetic storm, the plasma bubble is a very common phenomenon in the low latitude and equatorial ionosphere. Plasma bubbles occur almost every night in particular seasons with high solar activity. This much more frequent occurrence of the plasma bubble than the SED may require careful treatment.

Thus, the plasma bubble could be a serious threat to the GBAS in the magnetic low latitude region. Among the two major effects of the plasma bubble on GNSS, the ionospheric gradient and scintillation, the ionospheric gradient is more serious problem, because satellite lock-off would not be an integrity risk, while the ionospheric gradient may lead to misleading information to airborne users. General characteristics of the plasma bubble have been extensively studied for more than 30 years and are quite well known, except for day-to-day variability of the plasma bubble occurrence. However, precise observations of the spatial gradient of the ionospheric delay associated with the plasma bubble are not enough to characterize them. In such cases, modeling study based on the accumulated scientific knowledge is suitable. For this reason, [Saito et al., 2009] started developing a three-dimensional ionospheric delay model for the GBAS. They succeeded in reproducing a temporal variation of the ionospheric delay associated with a plasma bubble and modeling the satellite range correction errors.

We have extended the model to simulate the GBAS. Now the position domain errors associated with the plasma bubble can be estimated. In this study, GBAS simulations are extensively conducted with various conditions and some insight to what the worst case is for the plasma bubble threat is given.

2 PLASMA BUBBLE

The plasma bubble is a low-latitude and equatorial ionospheric phenomenon where the low density plasma in the bottom-side ionosphere explosively rises to the topside.

It is widely accepted that the basic process is the Rayleigh-Talyor plasma instability [Woodman and La Hoz, 1976]. Some characteristics of the plasma bubble important for the GBAS are summarized below.

- **Shape**
  The plasma bubble has a very characteristic three-dimensional structure. The shape of the plasma bubble is aligned with the earth's magnetic field lines. It is a cleft of the ionosphere with a fan-like shape extended in north-south and very thin in east-west (Fig. 1). Therefore, it is tallest over the magnetic equator, and the latitudinal extent is determined by the top altitude at the magnetic equator. The equatorial top altitude can often be as high as 1000 km (equivalent to 21.6 mag. lat. at 300 km altitude), and sometimes reach as high as 1500 km (equivalent to 25.9 mag. lat. at 300 km altitude).

- **Plasma density variation**
  Inside the plasma bubble, plasma density is extremely lower than that of outside. The boundary is very sharp, and the local plasma density changes 100 % to less than 10 % within a few tens kilometer [Burke et al., 2004a]. Therefore, the total number of electrons (TECs) along a satellite–receiver path to which the ionospheric delay is proportional also changes very sharply at the boundary of the plasma bubble. Since there are some plasmas above the plasma bubble (the topside ionosphere and the plasmasphere, generally 10–30 % contribution to the total delay), the ionospheric delay cannot be decreased down to zero. It should also be noted that the plasma bubble generally has a complex shape, the horizontal scale length of the ionospheric delay variation associated with the plasma bubble would be longer than that of the local plasma density variation.

- **Multiple bubble occurrence**
  Multiple plasma bubbles often occur with separation of about several hundred kilometers [Tsunoda, 2005, Fukao et al., 2006, Saito et al., 2008b]. Sometimes a single plasma bubble is generated. But it is often the case that two or more plasma bubbles are observed in the receiver field of view.

- **Drift**
  In general, the plasma bubble is generated at the sunset of the magnetic equator [Yokoyama et al., 2004], and drifts eastward typically at 50–150 m sec^{-1}. It is fastest around 20 LT and slows down as local time becomes late [Terra et al., 2004, Fukao et al., 2006, Yao and Makela, 2007]. Sometimes a plasma bubble

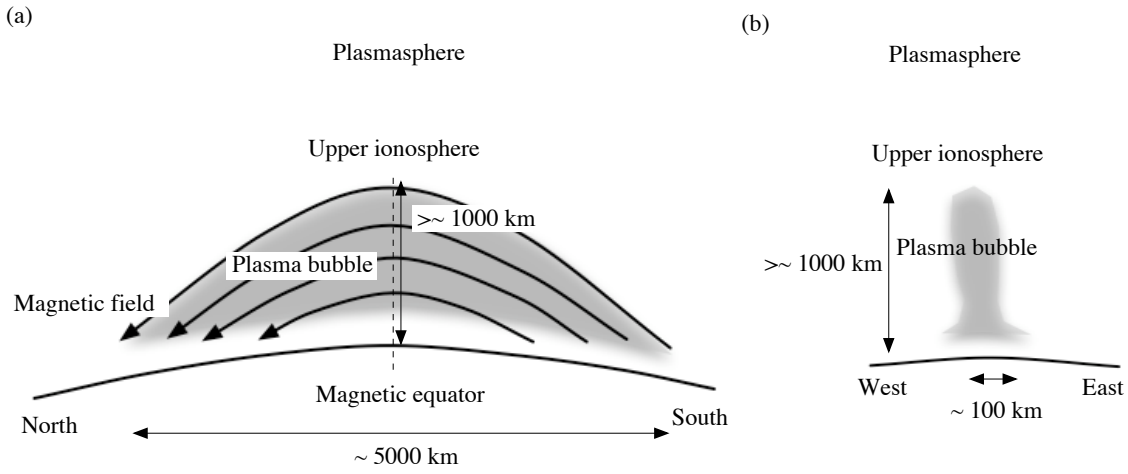

Figure 1. Illustration of the plasma bubble shape in (a) meridonal and (b) zonal planes.

stops with respect to the ground [Saito et al., 2008a]. During a magnetic storm, however, it can occur at any time from sunset to sunrise, and may drifts westward. Since the plasma bubble drifts almost together with the background thermospheric neutral wind, the zonal drift velocity is limited and not so fast as SEDs.

- **Occurrence: Solar activity dependence**
  The occurrence of the plasma bubble varies significantly with the solar activity. It occurs very often during the high solar activity period, while not often during the low solar activity period [Huang et al., 2002].

- **Occurrence: Season/Longitude dependence**
  The seasonal variation of the plasma bubble occurrence is closely related to the longitudinal variation. [Maruyama and Matuura, 1984, Burke et al., 2004a] The occurrence has two peaks around March and September equinoxes in Asian sector, while around November–February in the Atlantic sector.

- **Occurrence: Magnetic activity dependence**
  Unlike SEDs, many of plasma bubbles occur in magnetic quiet condition. According to satellite observations [Huang et al., 2001], the occurrence rate decreases as magnetic activity increases up to a moderately disturbed condition. In severely disturbed conditions, the occurrence rate increases with increasing magnetic activity. Since such severe magnetic conditions are not so common, majority of plasma bubbles occur in magnetic quiet conditions. (The magnetic disturbance and the ionospheric disturbance are not the same thing.) This should be kept in mind when we pick up observed data sets for analysis.

3 MODEL DESCRIPTIONS

The simplest way to model effects of plasma bubbles on the ionospheric delay is to use a two-dimensional ionospheric delay model and impose depletions due to plasma bubbles. Such 2-D models assume that the ionospheric delay comes from a virtual thin layer at a certain altitude around the ionospheric F region peak (∼300 km) and delay along a certain satellite–receiver path is represented by the virtual delay at a point at which the path crosses the virtual thin layer (an ionospheric pierce point, IPP). However, the plasma bubble has a three-dimensional structure constrained by the magnetic field. It is narrow in the east-west direction (∼100 km) and very elongated in the north-south direction (∼a few 1000 km). Furthermore, contribution of the upper ionosphere and the plasmasphere to the total delay could amount up to 30 % of the total delay which can be significantly different for different satellite–receiver paths which pass the same IPPs. Therefore, difference between ionospheric delays along the line of sights passing the same points in the virtual thin layer can be significant. For this reason, we develop a model where both the background ionosphere and plasma bubbles are described in a three-dimensional space.

Our model consists of a background ionospheric model and a plasma bubble. As a background ionospheric model, we use NeQuick [Giovannni and Radicella, 1990,Radicella and Zhang, 1995] where plasma density distribution between two arbitrary points. A plasma bubble model is defined in the vertical plane in the magnetic equator given as relative depletion compared with background. By defining the plasma bubble shape in the magnetic equatorial plane and utilizing high magnetic conjugacy of the plasma bubble [Otsuka et al., 2002], the plasma bubble shape can be defined in the 3-D space. The earth's magnetic field is approximated by the tilted-dipole model.

The background ionosphere is characterized by the

following parameters:

- geographic latitude, longitude, and altitude
- date and time in UT
- solar activity in terms of the solar radio flux index (F10.7) or the sunspot number index

So far, very simple plasma bubble shape, a rectangular, in the magnetic equatorial vertical plane are used. The plasma bubble moves zonally at a constant velocity. During the drift, it is assumed to keep the same shape. A tilted-dipole magnetic field model is used to trace magnetic field line from an arbitrary point to the magnetic equatorial vertical plane. Parameters that have been implemented to characterize plasma bubbles are as follows:

- number of plasma bubbles
- positions at the magnetic equator
- maximum depletion level relative to the background
- height at the magnetic equator
- zonal width
- scale length of the plasma bubble boundary
- zonal drift velocity

Plasma bubble characteristics which have not been implemented and will be implemented soon are as follows:

- use of the international geomagnetic reference field (IGRF) model
- arbitrary plasma bubble shape in the magnetic equatorial vertical plane
- scintillation presence (exists or not)

4 SIMULATION, RESULTS AND DISCUSSION

Positioning errors due to plasma bubbles are varies with various parameters, solar activity, season, airport location, satellite geometry, shape and location of the plasma bubble, approach path of airplanes, and so on. The number of combinations of different parameters are so huge that we first fix most of parameters and try changing some important parameters. Basic simulation parameters which are fixed throughout this study are summarized in Table 1. High solar activity, and March equinox season when the background ionospheric density is highest though a year to look for the worst case scenario associated with plasma bubbles. Since the plasma bubble is the nighttime phenomenon, the local time is 20 LT (11 UT) which is just after sunset when the background ionosphere is still dense. Figure 2a shows the zonal-altitudinal cross section of the ionospheric electron density over the magnetic equator. The vertical ionospheric delay distribution with the plasma bubble at 133.7°E at the magnetic equator is shown in Figure 2b. GBAS ground reference station is located at 25°N, 135°E which is at the poleward edge of the equatorial anomaly and in Japanese longitude. To see the effects of the plasma bubble more clearly, a single plasma bubble is considered in this simulation. The plasma bubble parameters are chosen to be of typical (not extreme) plasma bubbles. The RTCA standard 24 satellites [RTCA/DO-229D] are used. An airplane flies at 80 m sec^{-1} toward the GBAS reference station, and the simulation stops when the airplane come to the reference station. Range correction errors of each satellite and resulted positioning errors are calculated every 10 sec. Vertical protection levels are also calculated with typical σ values. To see the pure impact of the plasma bubble, no monitor, such as the code-carrier divergence monitor, is used in this simulation.

Table 1. Basic Parameters of simulation.

Background ionosphere	
Solar radio flux index (F10.7)	170 (high solar activity)
Season	March equinox
Local time	20 LT (11 UT)
Plasma bubble	
Zonal width	100 km
Depletion level	100 %
Equatorial height	800 km
Scale length of boundary	20 km
Eastward velocity	100 m s^{-1}
Reference station	
location	25°N, 135°E
Carrier-smoothing time constant	100 sec
Satellites	
Constellation	RTCA standard 24 satellites
Elevation mask	5°

In the following subsections, simulation results with different satellite geometry, different initial positions of a plasma bubble, and different approach directions. Conditions of each simulation are summarized in Table 2.

4.1 Simulation 1: Satellite geometry

In this simulation, airplane is initially located at about 40 km west of the GBAS reference station and the plasma bubble is located at 130 km west of the reference station and moves eastward at 100 m sec^{-1}. The simulation is conducted for 240 sets of satellite positions equivalent to changing ephemeris time-of-epoch every 6 minutes. Figure 3 shows an example of the simulation results in which the worst vertical error at 6 km from the GBAS reference station is obtained. The vertical error at 6 km from the GBAS reference station is +8.8 m. The positive vertical error means that the obtained position is higher than the true position and there is less distance between the airplane and the ground than

Table 2. Simulation conditions.

	Satellite geometry	Initial plasma bubble location	Approach direction
Sim. 1	Variable	133.7°E	Eastward (Runway 09)
Sim. 2	Worst case of Sim. 1	Variable	Eastward (Runway 09)
Sim. 3	Variable	133.7°E	Variable

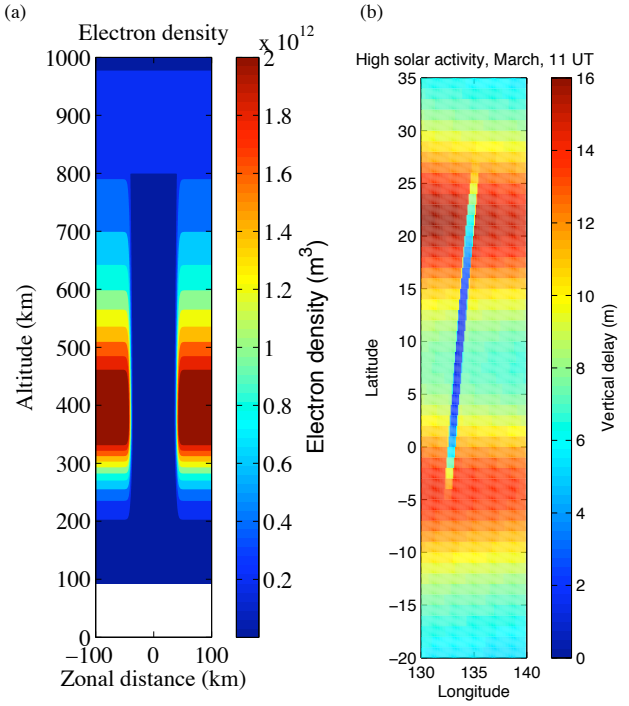

Figure 2. (a) Zonal-altitudinal cross section of the electron density over the equator with parameters in Table 1. (b) Vertical ionospheric delay at the L1 frequency with the plasma bubble at 133.7°E at the magnetic equator.

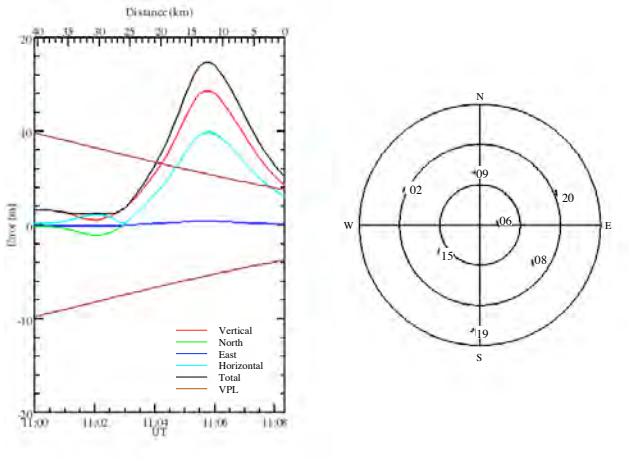

Figure 3. Left: The simulation results with the worst vertical errors at 6 km from the GBAS reference station. Red, green, blue, cyan, and black lines show the positioning errors in the east, north, and vertical (upward) directions and the total error, respectively. Brown line shows the vertical protection level. Right: Skyview plot of the satellite positions. Concentric circles show the elevation angles of 0, 30, and 60°.

estimated, which is more dangerous than the negative error case.

The right panel of Figure 3 shows the satellite positions in a skyview plot. Satellite-by-satellite range error analysis (not shown here) shows that the Sat. 19 experienced about 21 m range error at about 15 km from the GBAS reference station, and the range error at 6 km is still more than 10 m. Sat. 6 is also influenced slightly, but the range error at 6 km is almost zero. This means that the positioning errors are mostly due to the range error in Sat. 19. Although only one satellite is impacted by the plasma bubble, the resulted vertical error is quite significant.

4.2 Simulation 2: Plasma bubble position

In this simulation, airplane is initially located at about 40 km west of the GBAS reference station as Simulation 1. Satellite positions which gives the worst vertical error in Simulation 1 is used. The simulation is conducted various initial plasma bubble positions from 130°E to 139.9°E. This

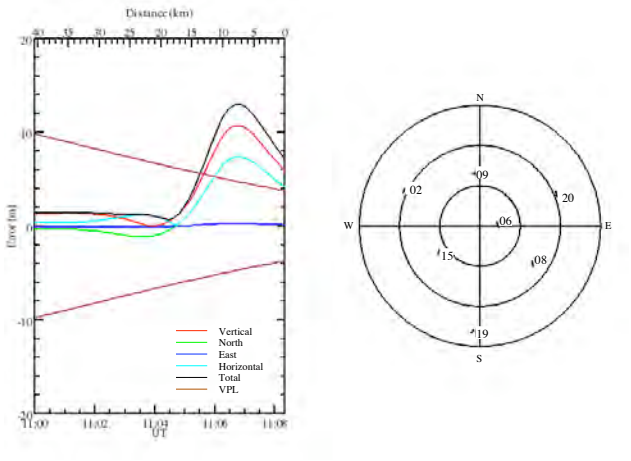

Figure 4. Same as Figure 3, but for the plasma bubble location which gives the worst vertical errors.

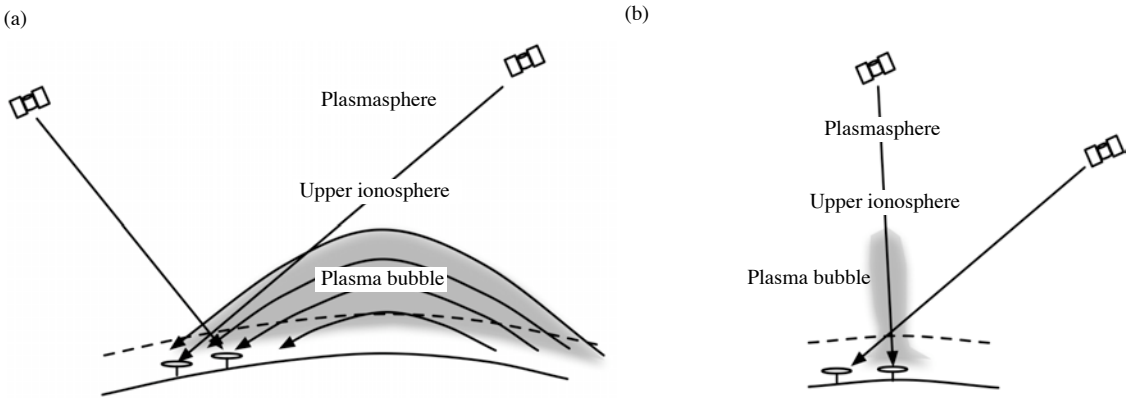

Figure 5. Satellite path and delay due to plasma bubble in (a) meridonal and (b) zonal planes.

simulation aims at investigating plasma bubble impact with different relative locations of the GBAS reference station, the airplane, and the plasma bubble. Figure 4 shows the results of the simulation in which the plasma bubble is initially located at 133.63°E and the vertical error at 6 km from the GBAS reference station is +10.2 m.

As Sim. 1 case, only Sat. 19 is impacted by the plasma bubble. For other initial plasma bubble locations, other satellites are also impacted just slightly. Sat. 19 is located to the south of the reference station at low elevation. Plasma bubble is alined in north-south slightly tilted in east-west due to magnetic declination. The satellite–receiver path of Sat. 19 is closely aligned with the plasma bubble edge and the ionospheric delay can change drastically between the GBAS reference station and the airplane (Figure 5b). In contrast, satellite–receiver path in the east or west directions pass across the plasma bubble, the ionospheric delay can change little. Thus, the satellites near the meridian of the GBAS reference station and the airplane should be more severely impacted by the plasma bubble. In this simulated case, there are Sat. 6 and Sat. 9 near the meridian. However, they are not or just slightly impacted. Sat. 9 is located too north and the satellite–receiver path is outside the plasma bubble. The satellite–receiver path of Sat. 6 passes indeed the plasma bubble. However, the path length inside the plasma bubble is much shorter than that of Sat. 19, and the amplitude of delay variation is small as it can be seen in Figure 5a.

These features cannot be expressed with 2-D ionospheric models and can be realized only by using a 3-D ionospheric model. It should be noted that real plasma bubbles generally have more complex shape than assumed in our model. It is also known that the plasma bubble tends to be inclined westward with the altitude. This means that it is also inclined westward with the magnetic latitude. And therefore we cannot simply exclude the possibility that satellites in the east or west at low elevation angles are impacted by plasma bubbles. However, the probability that those satellites are significantly impacted could be reduced.

4.3 Simulation 3: Approach direction

In this simulation, the plasma bubble is again located is located at 130 km west of the GBAS reference station. To investigate the effects of the approach direction, the simulation is conducted for four approach directions, northward (Runway 36), eastward (Runway 09), southward (Runway 18), and westward (Runway 27). For each approach direction, 240 satellite positions as Simulation 1 are used for this simulation. Figures 6a–d shows the results of the simulation with different satellite positions in which the worst vertical errors are obtained for Runway 36, 09, 18, and 27, respectively. For Runways 36 and 18, the maximum vertical errors at 6 km from the GBAS reference station are only 0.4 and 0.6 m, respectively, while they are +8.2 and -7.8 m for Runways 09 and 27.

In this simulation, the plasma bubble is assumed to develop vertically in the magnetic equatorial plane. This corresponds to the plasma bubble development along the magnetic meridian in the horizontal plane. For northward and southward approaches, the gradient associated with the plasma bubble impacts the satellite-receiver paths of the reference station and the airplane at the same time. This gives very small range correction error and results in small positioning error. Although real plasma bubbles have complex shapes, they are generally stretched long in the north-south direction and the ionospheric gradient tends to point the east-west direction. Therefore, GBAS for a runway aligned in north-south may be more resistant to the impact of the plasma bubble.

5 CONCLUSION

We have developed a three-dimensional ionospheric delay model with plasma bubbles and a simulation code to estimate the impact of the plasma bubble on GBAS.

Our simulation results show that a single plasma bubble can cause a positioning error in vertical more than 10 m. This means that the plasma bubble has a significant impact on plasma bubbles, and need to be detected by ground or airborne monitors. Currently our simulation does not in-

clude any monitors. But our simulation code is flexible to include such monitors easily, and we are working on implementing monitors such as a code-carrier-divergence monitor or an airborne monitor to compare 30 sec and 100 sec carrier-smoothed codes.

It is found that the impact of the plasma bubble is more significant when it comes around the meridian of the reference station, and not significant when it is located far east or west of the reference station. This result can be obtained only with a 3-D model which takes the plasma bubble structure into account.

Due to the north-south stretched shape of the plasma bubble, GBAS for a runway aligned in north-south is more resistant to the plasma bubble impact. To test with a plasma bubble with more realistic complex shape, we are working on including plasma bubble shapes observed with a multi-beam VHF backscatter radar.

Our model allows many parameters to be changed, and could be used not only for GBAS but also for SBAS or other applications.

REFERENCES

Burke, W. J., C. Y. Huang, L. C. Gentile, and L. Bauer, Longitudinal variability of equatorial plasma bubbles observed by DMSP and ROCSAT-1, J. Geophys. Res., 109, A12301, doi:10.1029/2004JA010583, 2004.

Fukao, S., Y. Ozawa, T. Yokoyama, M. Yamamoto, and R. T. Tsunoda, First observations of the spatial structure of F region 3-m-scale field-aligned irregularities with the Equatorial Atmosphere Radar in Indonesia, J. Geophys. Res., 109, A02304, doi:10.1029/2003JA010096.

Fukao, S., T. Yokoyama, T. Tayama, M. Yamamoto, T. Maruyama, and S. Saito, Eastward traverse of equatorial plasma plumes observed with the Equatorial Atmosphere Radar in Indonesia, Ann. Geophys., 24, 1411–1418, SRef-ID: 1432-0576/ag/2006-24-1411, 2006.

Di Giovanni, G. and S. R. Radicella, An analytical model of the electron density profile in the ionosphere, Adv. Space Res., 10, 27–30, 1990.

Huang, C. Y., W. J. Burke, J. S. Machuzak, L. C. Gentile, and P. J. Sultan, DMSP observations of equatorial plasma bubbles in the topside ionosphere near solar maximum, J. Geophys. Res., 106, 8131–8142, 2001.

Huang, C. Y., W. J. Burke, J. S. Machuzak, L. C. Gentile, and P. J. Sultan, Equatorial plasma bubbles observed by DMSP satellites during a full solar cycle: Toward a global climatology, J. Geophys. Res., 107, 1434, doi:10.1029/2002JA009652, 2002.

Maruyama, T., and N. Matuura, Longitudinal variability of annual changes in activity of equatorial spread F and plasma bubbles, J. Geophys. Res., 89, 10903–10912, 1984.

Otsuka, Y., K. Shiokawa, T. Ogawa, and P. Wilkinson, Geomagnetic conjugate observations of equatorial airgrow depletions, Geophys. Res. Lett., 29, 1753, doi:10.1029/015347, 2002.

Radicella, S. M. and M. L. Zhang, The improved DGR analytical model of electron density height profile and total electron content in the ionosphere, Annali di Geofisica, 38, 35-41, 1995.

RTCA/DO-229D, Minimum operational performance standards for global navigation system/wide area augmentaion system airborne equipment, December 13, 226.

Saito, S., S. Fukao, M. Yamamoto, Y. Otsuka, and T. Maruyama, Decay of 3-m-scale ionospheric irregularities associated with a plasma bubble observed with the Equatorial Atmosphere Radar, J. Geophys. Res., doi:10.1029/2008JA013118, 2008a.

Saito, S., T. Maruyama, M. Ishii, M. Kubota, G. Ma, Y. Chen, J. Li, C. Ha Duyen, and Thanh Le Truong, Observations of small- to large-scale ionospheric irregularities associated with plasma bubbles with a transequatorial HF propagation experiment and spaced GPS receivers, J. Geophys. Res., doi:10.1029/2008JA013149, 2008b.

Saito, S., T. Yoshihara, and N. Fujii, Development of an ionospheric delay model with plasma bubbles for GBAS, Proceedings of ION 2009 International Technical Meeting, 2009.

Terra, P. M., J. H. A. Sobral, M. A. Abdu, J. R. Souza, and H. Takahashi, Plasma bubble zonal velocity variations with solar activity in the Brazirian region, Ann. Geophys., 22, 3123–3128, 2004.

Tsunoda, R. T., On the enigma of day-to-day variability in equatorial spread F, Geophys. Res. Lett., 32, L08103, doi:10.1029/2005GL022512, 2005.

Yao, D., and J. J. Makela, Analysis of equatorial plasma bubble zonal drift velocities in the Pacific sector by imaging techniques, Ann. Geophys., 25, 701–709, 2007.

Yokoyama, T., S. Fukao, and M. Yamamoto, Relationship of the onset of equatorial F region irregularities with the sunset terminator observed with the Equatorial Atmosphere Radar, Geophys. Res. Lett., 31, L24804, doi:10.1029/2004GL021529, 2004.

Woodman, R. F., and C. La Hoz, Radar observations of F-region equatorial irregularities, J. Geophys. Res., 81, 5447-5466, 1976.

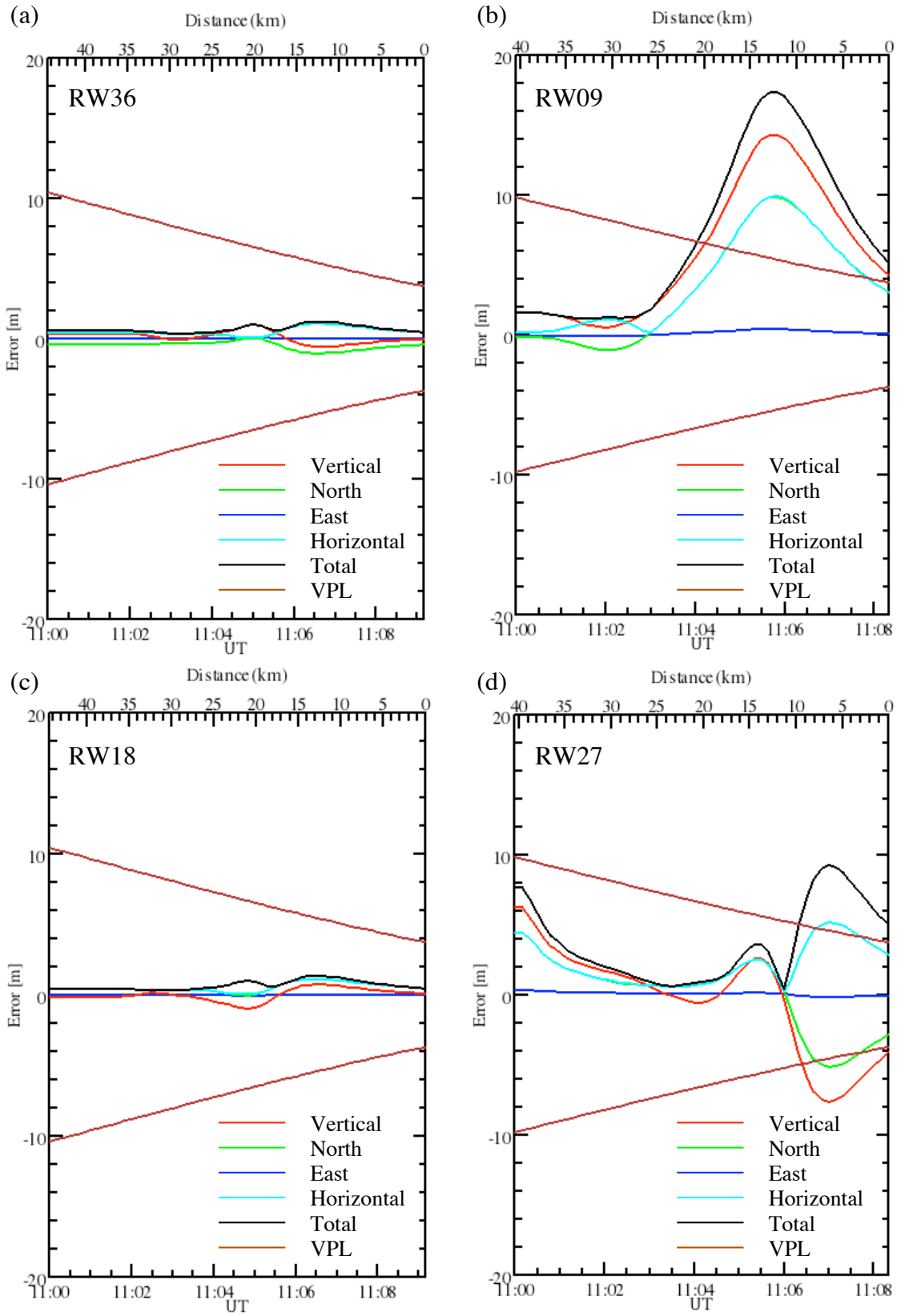

Figure 6. Same as Figure 3, but for the satellite positions with the worst vertical errors for the four approach directions. (a)–(d) correspond to Runway 36, 09, 18, and 27, respectively.

ATTACHMENT 2

Saito, S., T. Maruyama, M. Ishii, M. Kubota, G. Ma, Y. Chen, J. Li, C. Ha Duyen, and T. Le Truong, Observations of small- to large-scale ionospheric irregularities associated with plasma bubbles with a transequatorial HF propagation experiment and spaced GPS receivers, J. Geophys. Res., 113, A12313, doi:10.1029/2008JA013149, 2008.

JOURNAL OF GEOPHYSICAL RESEARCH, VOL. 113, A12313, doi:10.1029/2008JA013149, 2008

Observations of small- to large-scale ionospheric irregularities associated with plasma bubbles with a transequatorial HF propagation experiment and spaced GPS receivers

Susumu Saito,[1,2] Takashi Maruyama,[1] Mamoru Ishii,[1] Minoru Kubota,[1] Guanyi Ma,[3] Yanhong Chen,[4] Jinghua Li,[3] Chau Ha Duyen,[5] and Thanh Le Truong[5]

Received 7 March 2008; revised 1 October 2008; accepted 8 October 2008; published 30 December 2008.

[1] The results from simultaneous observations of the nighttime transequatorial propagation (TEP) of HF radio waves between Australia and Japan and the GPS scintillation measurements in south China and Vietnam are presented in this paper. The results showed that there was good correspondence between the nighttime eastward traveling off–great circle propagation (OGCP) of broadcasting waves of Radio Australia from Shepparton, Australia, measured at Oarai, Japan, and the scintillations in GPS radio waves at Hainan, China. This shows that the nighttime eastward traveling OGCP in HF TEP is caused by a large-scale ionospheric structure associated with a plasma bubble. The zonal drift velocities of the large-scale ionospheric structure estimated by the change in the direction of arrival of the OGCP were similar to those of the small-scale irregularities associated with plasma bubbles measured by the GPS scintillation spaced-receiver technique. Our results show that the HF TEP measurement is quite useful for monitoring the plasma bubble occurrence over a wide area and for forecasting the arrival of the plasma bubble at places located to the east of it.

Citation: Saito, S., T. Maruyama, M. Ishii, M. Kubota, G. Ma, Y. Chen, J. Li, C. Ha Duyen, and T. Le Truong (2008), Observations of small- to large-scale ionospheric irregularities associated with plasma bubbles with a transequatorial HF propagation experiment and spaced GPS receivers, *J. Geophys. Res.*, *113*, A12313, doi:10.1029/2008JA013149.

1. Introduction

[2] The transequatorial propagation (TEP) of HF radio waves has been used to detect large-scale equatorial ionospheric irregularities. HF waves are sometimes received in the off–great circle directions. *Röttger* [1973] used the HF TEP between Lindau, Germany, and Tsumeb, Namibia, to detect large-scale wave structures propagating eastward in the evening. He also showed that these structures are associated with the equatorial spread *F. Maruyama and Kawamura* [2006] used a sophisticated direction-finding system in Japan to receive the TEP of broadcasted HF waves from Australia and found that there is an off–great circle propagation (OGCP) traveling eastward during the night. They assumed that the off–great circle HF TEP was due to large-scale ionospheric structures at the equator and estimated that the typical velocity was 200 m s^{-1}. They therefore were able to conclude that the nighttime eastward traveling OGCP was probably related to a plasma bubble by using the motion and characteristic seasonal variation of this occurrence (two maxima at the equinox) and that by monitoring these HF waves they could monitor plasma bubbles over a wide area. However, they did not have any other methods for detecting plasma bubbles and thus were unable to confirm the one-to-one correspondence between the OGCP in the HF TEP and plasma bubbles.

[3] Scintillations of satellite radio waves have been used to detect ionospheric irregularities. It is already known that plasma bubbles accompany plasma irregularities at various wavelengths. When VHF or UHF radio waves pass through a plasma bubble, their amplitudes and phases fluctuate because of Fresnel diffraction caused by the irregularities with a horizontal scale size of $\sqrt{2\lambda h}$, where λ is the wavelength of the radio wave and h is the height of the irregularity associated with the plasma bubble. Such fluctuations are observed on the ground as scintillation. Over the past 10 years, the scintillations of GPS satellite signals have been used not only to detect plasma bubbles but also to measure the drift velocity of the irregularities associated with the plasma bubbles using a spaced-receiver technique [*Valladares et al.*, 1996; *Kil et al.*, 2000; *Kintner et al.*, 2004; *Ledvina et al.*, 2004; *Otsuka et al.*, 2006]. In this technique, one can measure the drift velocity of irregularities with a horizontal scale size of $\sqrt{2\lambda h}$, which is about 300–400 m for the GPS L1 wave (1.57542 GHz) when h is 250–400 km. Since the strong electron density gradient and the intense plasma irregularities associated with plasma bubbles are crucial problems in satellite-based precise posi-

[1]National Institute of Information and Communications Technology, Koganei, Japan.
[2]Now at Electronic Navigation Research Institute, Chofu, Japan.
[3]National Astronomical Observatories, Chinese Academy of Sciences, Beijing, China.
[4]Center for Space Science and Applied Research, Chinese Academy of Sciences, Beijing, China.
[5]Hanoi Institute of Geophysics, Vietnamese Academy of Science and Technology, Hanoi, Vietnam.

0148-0227/08/2008JA013149$09.00

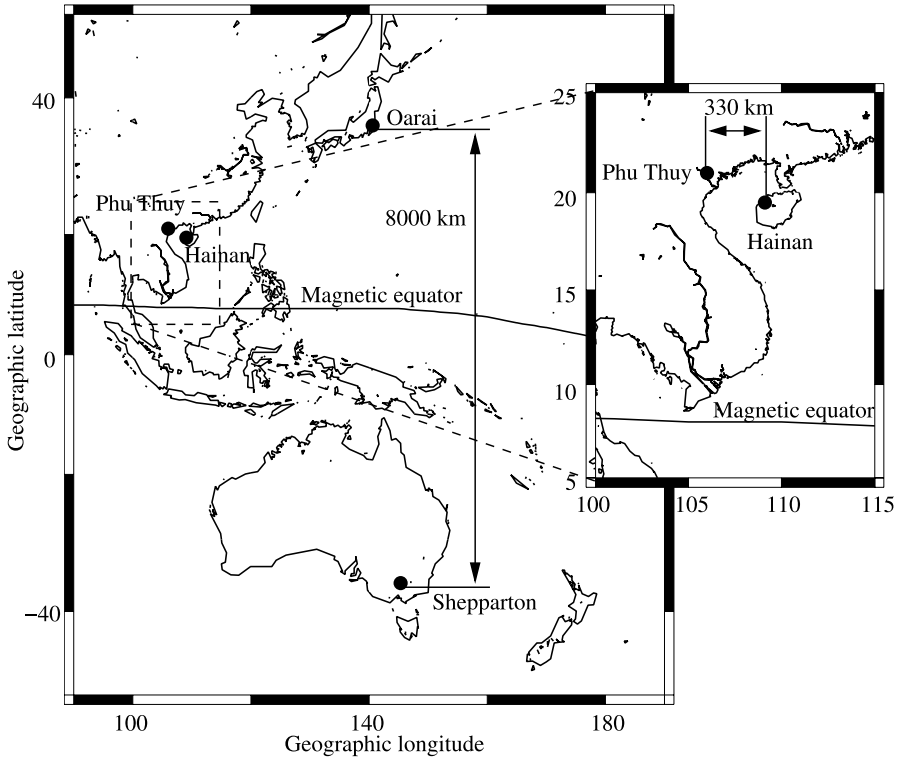

Figure 1. Experimental geometry.

tioning or satellite communications, it is very important to monitor the occurrence of plasma bubbles over a wide area and also to predict their movement.

[4] *Lin et al.* [2005] showed that there is a significant difference between the bulk zonal drift velocity of a plasma bubble measured by the IMAGE satellite and the plasma drift velocity measured in situ by the ROCSAT-1 satellite. They showed that the drift velocity of the plasma irregularities inside plasma bubbles that cause the scintillations of GPS radio waves may not necessarily be the same as the velocity of the large-scale structure of the plasma bubbles. This presents a problem when attempting to forecast the scintillation effects on radio systems by measuring the velocity of the plasma irregularities based on the GPS scintillation spaced-receiver technique. Thus, it is important to measure the plasma bubble–related velocities at different scale sizes using different techniques.

[5] The aim of the present study was to clarify what was observed in the HF TEP experiment, plasma bubbles or other matter, and to study the plasma bubble–related velocities at different scales by comparing the zonal velocity inferred from change of the direction of arrival (DOA) of the HF TEP with the velocity of plasma irregularities measured with the GPS scintillation spaced-receiver technique.

2. Observation

2.1. HF TEP

[6] HF broadcasting signals from Radio Australia transmitted from Shepparton, Australia (36.2°S, 145.3°E), are received at Oarai, Japan (36.3°N, 140.6°E). Shepparton and Oarai are at approximately the same meridian and are about 8000 km (Figure 1) from each other. They are located at roughly geographically conjugate points rather than magnetic conjugate points. At 140°E, the magnetic equator is at about 8°N. The azimuth angle in the great circle direction from Oarai to Shepparton is 175.7° measured clockwise from due north. The Oarai direction finder (ODF) consists of seven crossed-loop antennas 2 m in diameter that are located on a circle with a 60 m diameter. The multiple signal classification algorithm is used to determine the DOA (azimuth and elevation angles). The ODF can determine three different DOAs simultaneously with an angular resolution of 1° and a time resolution of 0.5 s [see *Maruyama and Kawamura*, 2006]. Although Radio Australia broadcasts 24 hours a day, the transmitted frequencies are changed depending on the local time and season. In our experiment, the receiving frequencies are scanned through all the possible frequencies. When the signals are found, the azimuth and zenith angles of the signals are measured for 8 s, and then the next frequency is observed.

[7] If we assume mirror reflection of the Radio Australia signal by a sharp plasma density gradient associated with a plasma bubble, it would be reflected around the geographic equator because Oarai is close to the geographic conjugate point of Shepparton. Since a plasma bubble extends from one hemisphere to the other [e.g., *Kelley et al.*, 2003; *Keskinen et al.*, 2003], the same plasma bubble should exist at the geographic equator along the same longitude as Hainan when the plasma bubble is observed at Hainan. The azimuth angle of the geographic equator along the same longitude as Hainan is 226° from Oarai (Figure 2). Of course, the Radio Australia signal may not only be reflected at the geographic equator. Nevertheless, OGCP around 226° could be detected as scintillations at Hainan if a plasma bubble responsible for the OGCP develops around the latitude of the field of view of

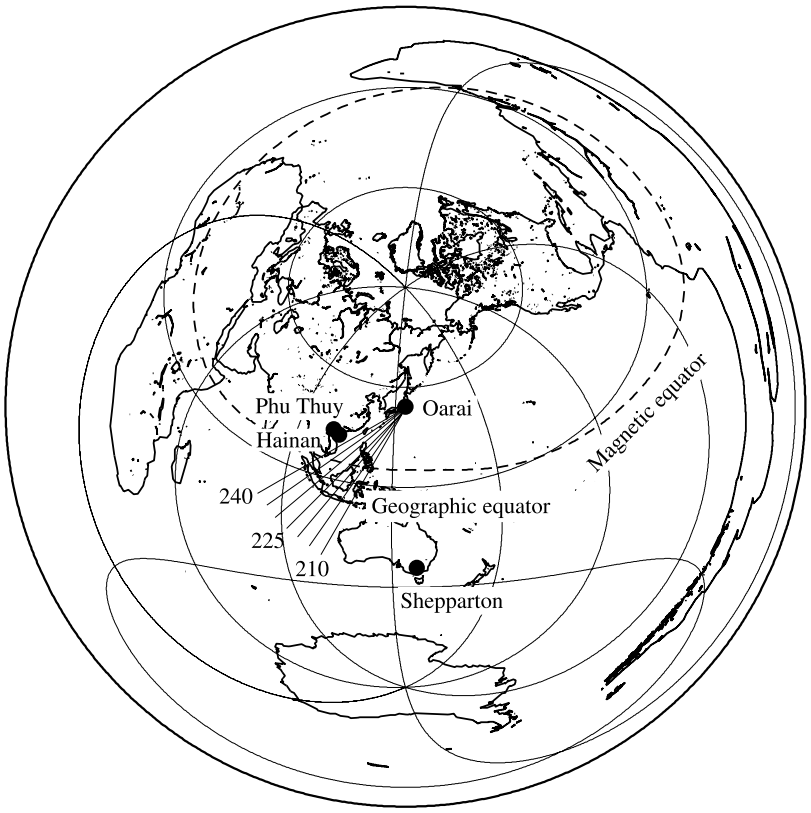

Figure 2. Azimuthal equidistant projection of directions of arrival (DOAs) in Oarai. The radial lines indicate the DOAs from 210° to 240° every 5° measured clockwise from due north.

Hainan. The footprint of a plasma bubble is often not aligned with the longitude. Furthermore, the wave may be reflected more than once. Therefore, it is inevitable that there will be some scattering of the azimuth angle around 226°.

2.2. GPS Scintillation

[8] The drift velocities of plasma irregularities associated with plasma bubbles were measured at Hainan, China (19.5°N, 109.1°E, +13.9° magnetic latitude), and Phu Thuy, Vietnam (21.0°N, 106.0°E, +15.7° magnetic latitude). Hainan and Phu Thuy are zonally separated by 330 km (Figure 1). At both sites, three GPS receivers were installed. Two Ashtech G12 receivers and one Ashtech BR2G receiver were installed in Hainan. The carrier-to-noise ratio (CNR) was sampled at 20 Hz. Three JAVAD LGG100 receivers were installed in Phu Thuy. The sampling rate of the CNR in Phu Thuy was 100 Hz. The specifications of the GPS receivers at both sites are summarized in Table 1. The three receiver antennas were located 90–100 m apart at each site. Figure 3 shows the distribution of the receiver antennas in Hainan and Phu Thuy. The S_4 scintillation index, the maximum values of the correlation functions between the CNR measured by each receiver, and the time lags corresponding to the maximum correlation are calculated every 60 s. The drift velocity of the scintillation pattern on the ground is estimated from the time lags between the signals of each receiver. This could lead to errors in the estimation of the velocity [*Briggs et al.*, 1950]. However, this effect can be neglected by using highly correlated data [*Kintner et al.*, 2004]. The zonal drift velocities of ionospheric irregularities are estimated from the drift velocity of the scintillation pattern on the ground and the satellite ephemeris on the basis of *Ledvina et al.* [2004]. The altitude of the ionospheric puncture point (IPP) is assumed to be 300 km. The shape of the irregularities is assumed to be aligned with the magnetic field line. According to *Ledvina et al.* [2004], the zonal drift velocity of the scintillation pattern on the ground (v_{scintx}) is given by

$$v_{scintx} = \frac{z_{sat}}{z_{sat} - z_{ion}} \left\{ v_{ionx} + (q_y/q_x) v_{iony} + (q_z/q_x) v_{ionz} - \frac{z_{ion}}{z_{sat}} \left[v_{satx} + (q_y/q_x) v_{saty} + (q_z/q_x) v_{satz} \right] \right\}, \quad (1)$$

where z_{sat} is the altitude of the satellite and z_{ion} is that of the ionosphere; v_{ionx}, v_{iony}, and v_{ionz} are the eastward, northward, and vertical components of the irregularity drift velocity in the receiver reference frame, respectively; v_{satx}, v_{saty}, and v_{isatz} are the magnetic eastward, northward, and vertical components of the satellite velocity, respectively; and q_x, q_y, and q_z are the geometrical coefficients determined by the geomagnetic field and the satellite direction [see *Ledvina et al.*, 2004, Appendix A]. The irregularity drift velocity in magnetic coordinates (x is magnetic east, and z is upward and perpendicular to the magnetic field) at the ionospheric puncture point ($\mathbf{v}_{ipp}$) is related to that in the local coordinates of the receiver $\mathbf{v}_{ipp}$ with a 3 × 3 transform matrix $\mathbf{R}$:

$$\mathbf{v}_{ipp} = \mathbf{R}\mathbf{v}_{ion}. \quad (2)$$

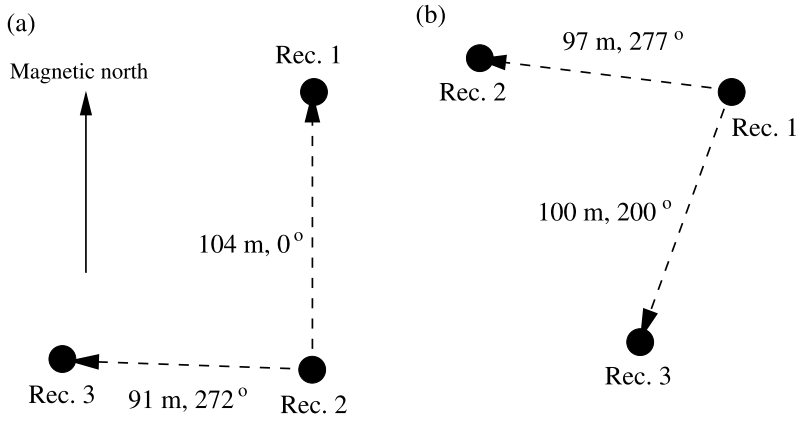

Figure 3. Distribution of GPS receiver antennas at (a) Hainan, China, and (b) Phu Thuy, Vietnam. The angles representing the relative positions of the antennas were measured clockwise from magnetic north.

The zonal and upward components of the irregularity drift velocity in magnetic coordinates at the IPP are given by

$$\begin{bmatrix} v_{ippx} \\ v_{ippz} \end{bmatrix} = \begin{bmatrix} R_{11} - \dfrac{R_{21}R_{12}}{R_{22}} & R_{13} - \dfrac{R_{21}R_{32}}{R_{22}} \\ R_{13} - \dfrac{R_{23}R_{12}}{R_{22}} & R_{33} - \dfrac{R_{23}R_{32}}{R_{22}} \end{bmatrix} \begin{bmatrix} v_{ionx} \\ v_{ionz} \end{bmatrix}, \quad (3)$$

where R_{ij} represents the (i,j) component of the matrix **R** given by *Ledvina et al.* [2004, equation (8)]. If we define a matrix **S** as

$$\mathbf{S} = \begin{bmatrix} R_{11} - \dfrac{R_{21}R_{12}}{R_{22}} & R_{13} - \dfrac{R_{23}R_{12}}{R_{22}} \\ R_{13} - \dfrac{R_{21}R_{32}}{R_{22}} & R_{33} - \dfrac{R_{23}R_{32}}{R_{22}} \end{bmatrix}^{-1}, \quad (4)$$

where $[\,]^{-1}$ denotes the matrix inversion, equation (1) becomes

$$v_{scintx} = \frac{z_{sat}}{z_{sat} - z_{ion}} \left\{ \left[\left(1 - \frac{q_y}{q_x}\frac{R_{21}}{R_{22}} \right) S_{11} + \left(\frac{q_z}{q_x} - \frac{q_y}{q_x}\frac{R_{23}}{R_{22}} \right) S_{21} \right] v_{ippx} \right.$$
$$\cdot \left[\left(1 - \frac{q_y}{q_x}\frac{R_{21}}{R_{22}} \right) S_{12} + \left(\frac{q_z}{q_x} - \frac{q_y}{q_x}\frac{R_{23}}{R_{22}} \right) S_{22} \right] v_{ippz}$$
$$\left. - \frac{z_{ion}}{z_{sat}} \left[v_{satx} + \frac{q_y}{q_x} v_{saty} + \frac{q_z}{q_x} v_{satz} \right] \right\}. \quad (5)$$

In our analysis, the meridional drift velocity of the irregularities (v_{ippz}) is assumed to be zero. This assumption may prove false when the drift velocity has a significant upward (vertical/meridional) component because the drift velocity of the scintillation pattern depends on the three-dimensional drift velocity of the irregularities as well as the satellite position. After a plasma bubble has been developed, however, the vertical drift velocity is generally small. According to *Fejer et al.* [1991], after the prereversal enhancement period, the vertical drift velocity is about 5 times slower than the zonal velocity. By selecting the data in which the contribution of the upward component to the scintillation drift velocity is much smaller than that of the zonal component, our assumption can be justified. In our analysis, only the data where the coefficient of v_{ippx} in equation (5) was more than 2 times larger than that of v_{ippz} were used, so the contribution of the upward component is 10 times smaller than that of the zonal component.

3. Results

[9] Figure 4 shows the azimuth angle of arrival (clockwise from due north) of the Radio Australia signal on 29 March 2007. The data group around 176°, which we call the "main trace" [*Maruyama and Kawamura*, 2006], is the signals of the great circle propagation. There are other data groups to the west of the main trace from 1200 to 1900 UT, which we call the "satellite traces." The angle decreases with time, showing that the reflection point was moving eastward. *Maruyama and Kawamura* [2006] assumed that this is due to the eastward motion of the large-scale equatorial ionospheric structure associated with the plasma bubble. Other data groups, such as those around 240° from 1030 to 1200 UT, 260° from 1400 to 1600 UT, or 260° from 1700 to 1800 UT, were found to be from radio sources other than Radio Australia. Using the method employed by *Maruyama and Kawamura* [2006], the eastward velocity of the ionospheric structure corresponding to the first slope in Figure 4 was derived as 93 m s^{-1} from the slope of the trace. The velocity estimation error associated with determining the slope is 7–8 m s^{-1} if the slope is perfectly determined. For diffuse traces, the error can be much larger.

[10] In the evening of the same day, strong scintillations of the GPS radio waves were observed in Hainan. Figure 5 shows the S_4 observed by the three receivers in Hainan. These large S_4 values were observed for the signals from PRN 16 and PRN 22 satellites from 1240 to 1315 UT and from 1315 to 1345 UT, respectively. At the same time, no scintillation was observed in Phu Thuy. Figures 6 and 7

Table 1. GPS Receiver System Specifications

Location	Hainan	Phu Thuy
Latitude	19.5°N	21.0°N
Longitude	109.1°E	106.0°E
Dip latitude	+13.9°	+15.7°
Receiver	Ashtech G12/BR2G	JAVAD LGG100
Frequency	L1 (1.57542 GHz)	L1 (1.57542 GHz)
Sampling rate	20 Hz	100 Hz

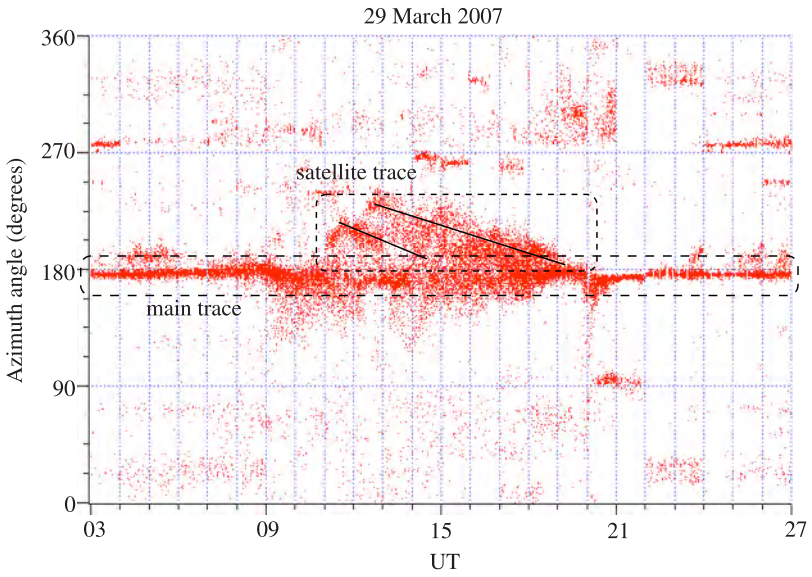

Figure 4. Azimuth angles of the Radio Australia signal measured by ODF on 29 March 2007. The angle was measured clockwise from due north.

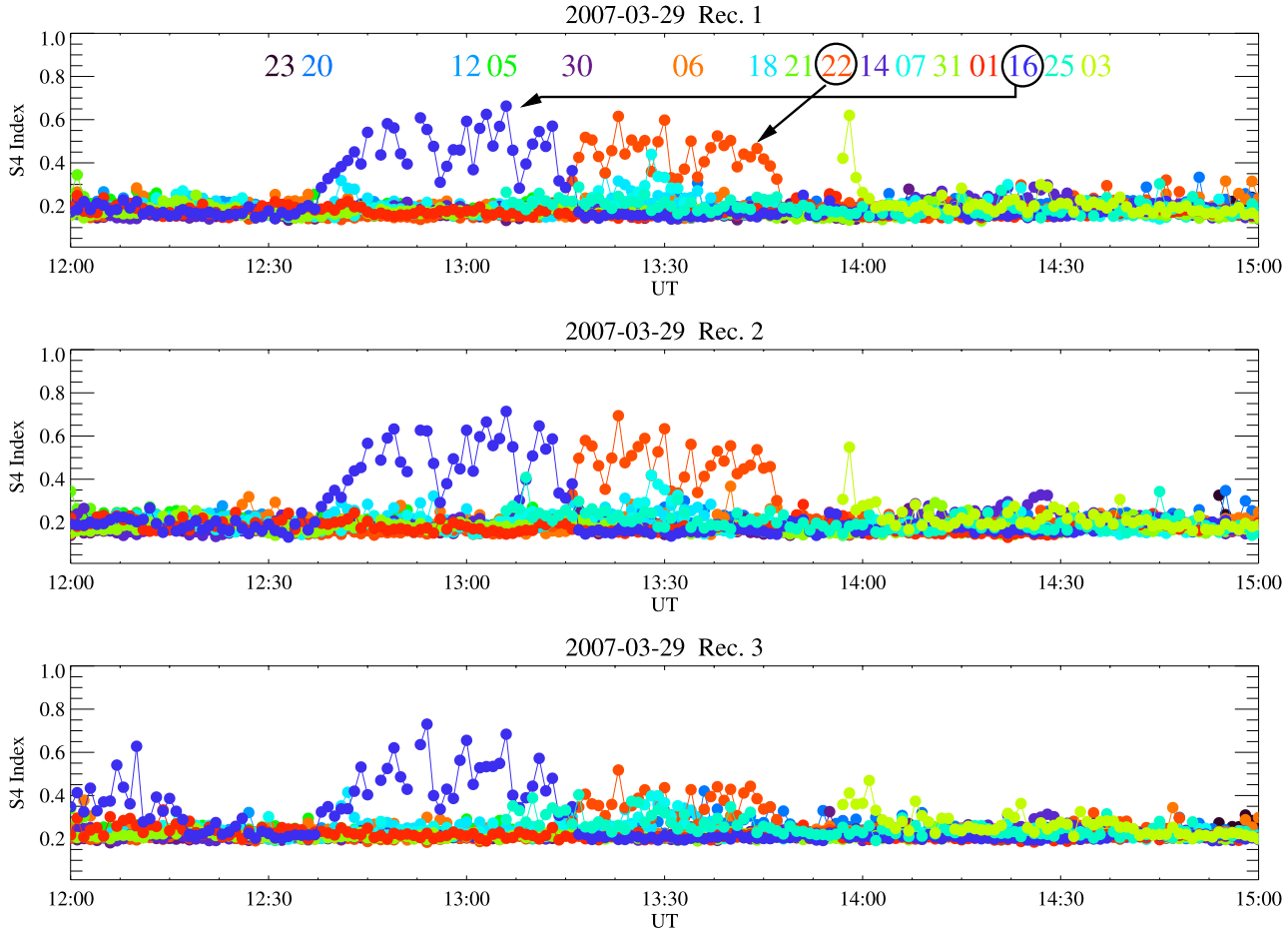

Figure 5. S_4 indices measured in Hainan on 29 March 2007. The different colors represent the different satellites indicated by numbers on the top plot.

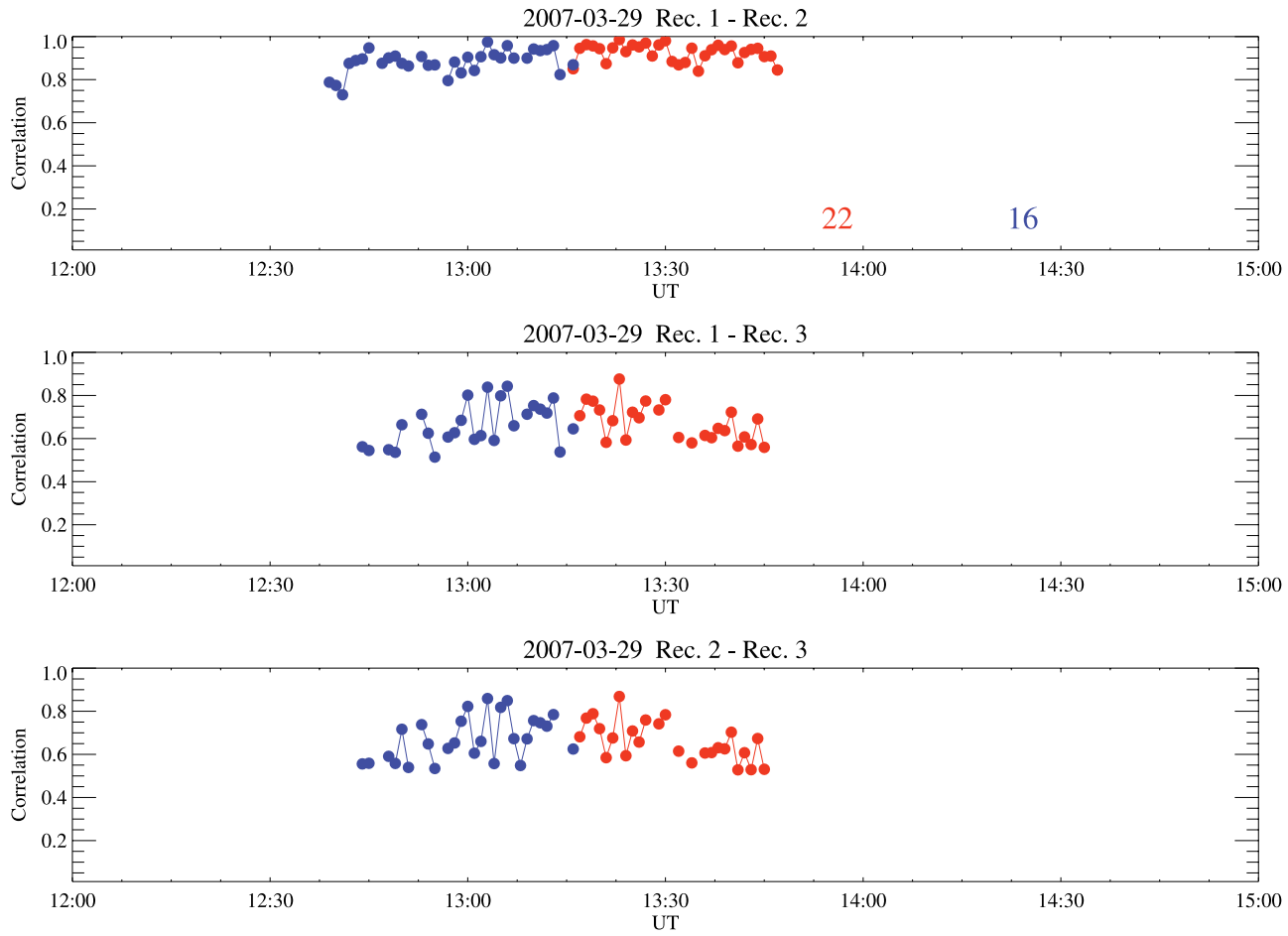

Figure 6. Correlation coefficients between temporal variations of CNR for the PRN 16 (blue) and PRN 22 (red) GPS satellites measured by each receiver in Hainan on 29 March 2007. Only the data with S_4 indices greater than 0.3 were used.

show the maximum correlation and corresponding time lags for all receiver combinations, respectively. Only the data where S_4 was greater than 0.3 were plotted. The correlation was generally high, and the correlation between receiver 1 and receiver 2 was especially high (>0.9). On the basis of the method by *Ledvina et al.* [2004] described in section 2.2, the drift velocity of the ionospheric irregularities were estimated (Figure 8) as about 130 m s^{-1} (eastward), which is similar to the average plasma drift velocity obtained by the Jicamarca radar [*Fejer et al.*, 1991]. Drift velocities could not be derived with the PRN 16 data because the coefficients of v_{ippx} and v_{ippz} in equation (5) did not satisfy our criterion that the contribution of v_{ippz} to v_{scintx} is 10 times smaller than that of v_{ippx}. The drift velocity measured by the GPS scintillation spaced-receiver technique reasonably agreed with the drift velocity deduced from the movement of the large-scale ionospheric structure observed by the HF TEP.

[11] The ODF observed an OGCP in the HF TEP around an azimuth of 226° on 26, 29, and 31 March; 18 September; and 22 October 2007. The Hainan GPS receiver system detected scintillations that were likely due to plasma bubbles on 26, 29, and 31 March; 1 and 15 April; 18 September; and 22 October 2007. The Phu Thuy GPS receiver system was not functioning properly, and thus, it was difficult to draw any conclusive results except for the data on 29 March 2007. Table 2 summarizes the OGCP occurrences in the HF TEP with DOAs around 226° and the GPS scintillations in Hainan and Phu Thuy. On 15 April 2007, the ODF recorded no data because of system maintenance. Table 3 summarizes the occurrence periods of the OGCP in the HF TEP with DOAs around 226° and the GPS scintillations in Hainan, which show the temporal correspondence between the OGCP in the HF TEP and the GPS scintillation. It can be seen from Tables 2 and 3 that the OGCP occurrence in the HF TEP is in very good agreement with that of the GPS scintillations. It should be noted that the OGCP started earlier and ceased later than the GPS scintillation at Hainan. This means that the HF TEP can observe a wider area than the GPS receivers at a single site.

4. Discussion

[12] The tracks of the ionospheric puncture points of GPS satellites at an altitude of 300 km seen from Hainan are shown in Figure 9a. The red curves in Figure 9a along the track show the intervals where scintillation was observed. Figure 9b is the same as Figure 9a except for the receiving site, which was at Phu Thuy. The red curves in Figure 9a are

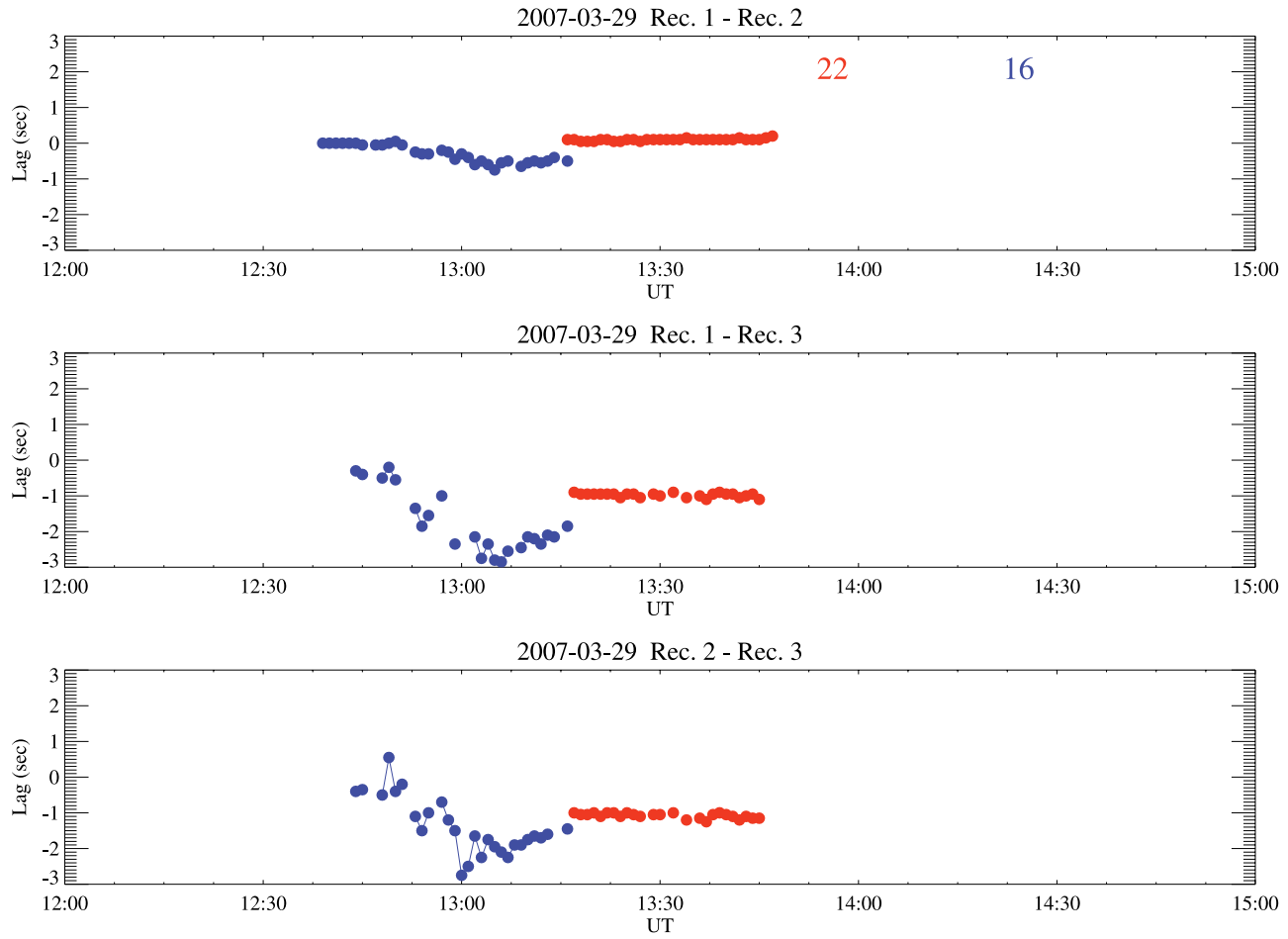

Figure 7. Time lags between temporal variations of CNR for the PRN 16 (blue) and PRN 22 (red) GPS satellites measured by each receiver in Hainan on 29 March 2007. Only the data with S_4 indices greater than 0.3 were used.

duplicated in Figure 9b. It can be seen that the satellite tracks seen from Phu Thuy did not encounter the locations where scintillation was observed at Hainan. The satellite PRN 18 seen from Phu Thuy was close to the scintillation interval of PRN 22 from Hainan but passed southeastward without encountering the plasma bubble. This explains why scintillation was not observed at Phu Thuy.

[13] As seen in Figure 5, the strong scintillation of PRN 16 ceased when the strong scintillation of PRN 22 started at Hainan. On the basis of this fact, the western and eastern edges of the plasma bubble that caused the scintillation could be estimated. If we assume that the shape and velocity of the plasma bubble do not change, the bulk velocity of the plasma bubble can be estimated. According to Figure 10, the plasma bubble traveled eastward about 2.5° in longitude

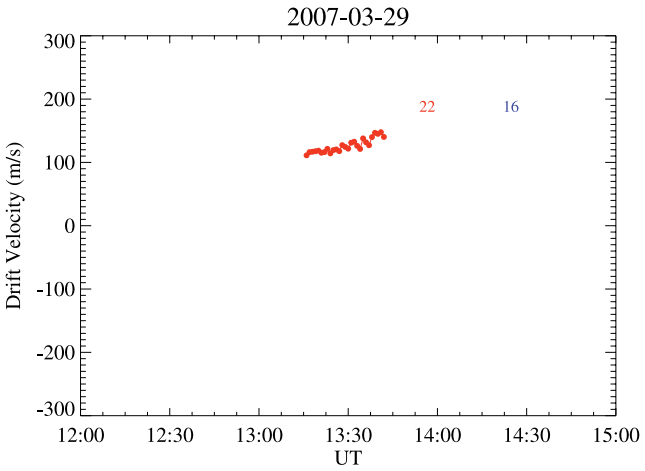

Figure 8. Estimated zonal drift velocity estimated for PRN 16 (blue) and PRN 22 (red) satellites in Hainan. Only the data with S_4 indices greater than 0.3 were used.

Table 2. OGCP Occurrences in the HF TEP and GPS Scintillation[a]

		GPS Scintillation	
Date	HF TEP OGCP, Oarai[b]	Hainan	Phu Thuy
26 March 2007	O	O	ND
29 March 2007	O	O	NO
31 March 2007	O	O	ND
15 April 2007	ND	O	ND
18 September 2007	F	O	ND
22 October 2007	O	O	ND

[a]O, NO, and ND indicate occurrence, no occurrence, and no data available, respectively. On 18 September 2007, the OGCP signal was very faint (represented by F).
[b]DOAs were around 226°.

Table 3. Occurrence Periods of the OGCP in the HF TEP and GPS Scintillation

Date	HF TEP, Oarai (UT)[a]	GPS Scintillation, Hainan (UT)
26 March 2007	1150–1530	1240–1500
29 March 2007	1130–1500	1240–1345
31 March 2007	1130–1700	1220–1400
18 September 2007	1445–1700	1430–1600
22 October 2007	1100–1400	1330–1355

[a]DOAs were around 226°.

in 30 min. If we assume that the plasma bubble kept the same shape and drifted at a constant velocity, the eastward drift velocity of the plasma bubble can be estimated to be 150 m s^{-1}, which is in good agreement with the irregularity drift velocity measured from the scintillation pattern measurements (~130 m s^{-1}). For the plasma bubble observed on 29 March 2007, the velocities of plasma bubble motion, the small-scale irregularities embedded in the plasma bubble, and the large-scale ionospheric structure observed with the HF TEP are all similar.

[14] Table 4 shows a comparison of the drift velocities measured using the HF TEP at Oarai with those from the GPS scintillation measurement at Hainan. On 18 September 2007, the drift velocity could not be derived from the HF TEP because the signal level was too low. On 22 October 2007, a reliable drift velocity could not be derived by the Hainan GPS receiver system because the satellite elevation angle was too low. The drift velocities measured by the ODF are in reasonable agreement with those simultaneously measured by the Hainan GPS receiver system. *Huba et al.* [2008] showed that the vertical $\mathbf{E} \times \mathbf{B}$ drift velocity inside plasma bubbles can be different from the velocity of the vertical development of plasma bubbles. Although it would be interesting to compare large-scale and small-scale dynamics related to plasma bubbles, the discrepancies between the velocities measured by the two techniques described in this paper are within the error in the measurements by the ODF. Thus, it is difficult to give a clear answer to the question raised by *Lin et al.* [2005] on the difference between the drift velocities of large-scale ionospheric structure and the small-scale irregularities. Nevertheless, it is a new finding that the OGCP in the HF TEP and GPS scintillation are observed simultaneously, and the derived drift velocities by the two techniques were found to be similar, even though there was only a small amount of simultaneous data. Our results support the hypothesis that the nighttime eastward traveling OGCP in the HF TEP is associated with plasma bubbles.

[15] For at least the three cases in which the drift velocities were simultaneously measured (Table 4), both the large-scale ionospheric structure and the 300–400-m-scale irregularities associated with the plasma bubble drifted together. HF radio waves would be reflected at the wall of the plasma bubble,

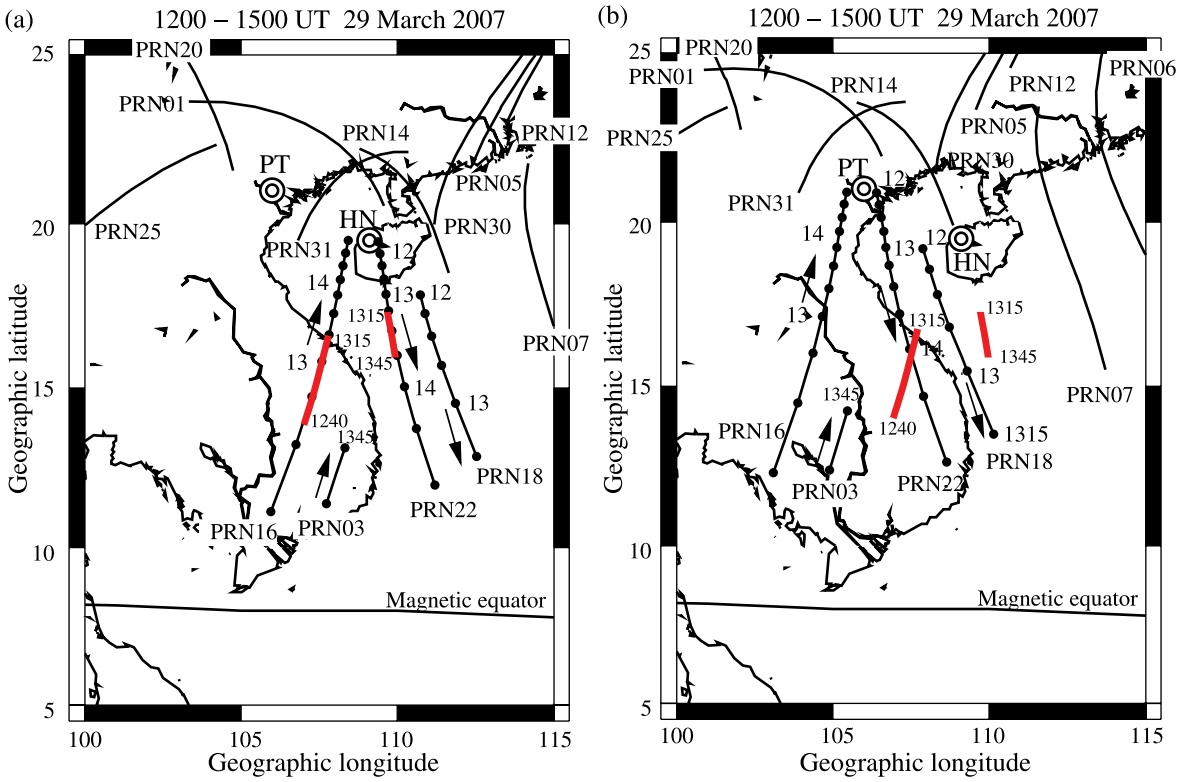

Figure 9. Tracks of satellites at an altitude of 300 km in (a) Hainan (HN) and (b) Phu Thuy (PT) from 1200 to 1500 UT on 29 March 2007. The dots on the tracks show the positions of the satellites mapped at an altitude of 300 km every 15 min. The numbers by the tracks indicate the time in UT. The red lines indicate the intervals where strong scintillations were observed in Hainan.

presumably around the *F* peak or below, when the OGCP in the HF TEP occurs. Since the intensity of scintillation is proportional to the absolute value of the electron density fluctuation, irregularities around the *F* peak would most significantly contribute to the scintillation of GPS radio waves. Thus, both of the techniques we used are sensitive to similar altitudes related to plasma bubbles and could measure similar drift velocities. The movement of the scintillation region for the data from 29 March 2007 (Figure 10) supports this conclusion.

5. Summary and Conclusion

[16] The data from an experiment where the HF TEP and the GPS scintillation were simultaneously measured for the first time were presented. The HF TEP of the broadcasting signal from Radio Australia in Shepparton, Australia, was measured at Oarai, Japan. Scintillations in the GPS radio waves were observed in Hainan, China, and at Phu Thuy, Vietnam. Although only a small amount of the GPS scintillation data in Phu Thuy was available, the scintillations in the GPS radio waves in Hainan corresponded well with the OGCP occurrences in the HF TEP in Oarai, with DOAs of around 226°. This means that the OGCP in the HF TEP is associated with a large-scale ionospheric structure associated with the plasma bubble. Furthermore, the zonal drift velocities of the large-scale ionospheric structure were similar to those of the 300–400-m-scale irregularities associated with plasma bubbles measured by the GPS scintillation spaced-receiver technique. Our results prove that the HF TEP measurement is very useful for monitoring plasma bubbles over a wide area and for forecasting the arrivals of plasma bubbles. In order to make more precise measurements of the locations and velocities of plasma bubbles, the uncertainties in the DOAs must be reduced, and the true propagation path must be identified. Locating transmitters designated for TEP experiments at higher frequencies in the VHF band may be desirable for the wide-area monitoring of plasma bubbles. Ranging the TEP path by measuring the propagation time from the radio source to the receiver by using a passive radar technique would also be useful.

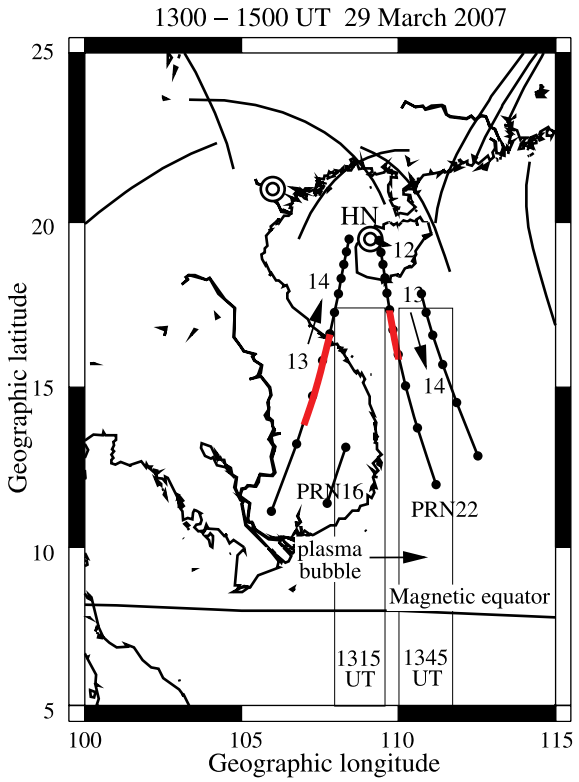

Figure 10. Similar to Figure 9a but for inferred locations of the plasma bubble at 1315 and 1345 UT.

Table 4. Zonal Drift Velocities Inferred From the HF TEP and the GPS Scintillation[a]

Date	HF TEP, Oarai (m s^{-1})	GPS Scintillation, Hainan (m s^{-1})
26 March 2007	77	80
29 March 2007	93	130
31 March 2007	93	80
15 April 2007	-	95
18 September 2007	-	50
22 October 2007	39	-

[a]The positive velocity refers to the eastward motion. The dash means that there was no observation or the data quality was too low to derive the velocity.

[17] **Acknowledgments.** The authors are grateful to Masabumi Kawamura for managing the Oarai Direction Finder data. This work forms a part of Southeast Asia low latitude ionospheric network (SEALION) project. The authors thank all those who participate in the SEALION project.

[18] Amitava Bhattacharjee thanks Yuichi Otsuka and another reviewer for their assistance in evaluating this paper.

References

Briggs, B. H., G. J. Philips, and D. H. Shinn (1950), The analysis of observations on spaced receivers of the fading of radio signals, *Proc. Phys. Soc., Ser. B*, *63*, 106–121.

Fejer, B. G., E. R. de Paula, S. A. Gonzaléz, and R. F. Woodman (1991), Average vertical and zonal F region plasma drifts over Jicamarca, *J. Geophys. Res.*, *96*, 13,901–13,908.

Huba, J. D., G. Joyce, and J. Krall (2008), Three-dimensional equatorial spread *F* modeling, *Geophys. Res. Lett.*, *35*, L10102, doi:10.1029/2008GL033509.

Kelley, M. C., J. J. Makela, L. J. Paxton, F. Kamalabadi, J. M. Comberiate, and H. Kil (2003), The first coordinated ground- and space-based optical observations of equatorial plasma bubbles, *Geophys. Res. Lett.*, *30*(14), 1766, doi:10.1029/2003GL017301.

Keskinen, M. J., S. L. Ossakow, and B. G. Fejer (2003), Three-dimensional nonlinear evolution of equatorial spread- *F* bubbles, *Geophys. Res. Lett.*, *30*(16), 1855, doi:10.1029/2003GL017418.

Kil, H., P. M. Kintner, E. R. de Paula, and I. J. Kantor (2000), Global Positioning System measurements of the ionospheric zonal apparent velocity at Cachoeira Paulista in Brazil, *J. Geophys. Res.*, *105*, 5317–5327.

Kintner, P. M., B. M. Ledvina, E. R. de Paula, and I. J. Kantor (2004), The size, shape, orientation, speed, and duration of GPS equatorial anomaly scintillations, *Radio Sci.*, *39*, RS2012, doi:10.1029/2003RS002878.

Ledvina, B. M., P. M. Kintner, and E. R. de Paula (2004), Understanding spaced-receiver zonal velocity estimation, *J. Geophys. Res.*, *109*, A10306, doi:10.1029/2004JA010489.

Lin, C. S., T. J. Immel, H.-C. Yeh, S. B. Mende, and J. L. Burch (2005), Simultaneous observations of equatorial plasma depletion by IMAGE and ROCSAT-1 satellites, *J. Geophys. Res.*, *110*, A06304, doi:10.1029/2004JA010774.

Maruyama, T., and M. Kawamura (2006), Equatorial ionospheric disturbance observed through a transequatorial HF propagation experiment, *Ann. Geophys.*, *24*, 1401–1409.

Otsuka, Y., K. Shiokawa, and T. Ogawa (2006), Equatorial ionospheric scintillations and zonal irregularity drifts observed with closely-spaced GPS receivers in Indonesia, *J. Meteorol. Soc. Jpn.*, *84A*, 343–351.

Röttger, J. (1973), Wave-like structures of large-scale equatorial spread-*F* irregularities, *J. Atmos. Terr. Phys.*, *35*, 1195–1206.

Valladares, C. E., R. Sheehan, S. Basu, H. Kuenzler, and J. Espinoza (1996), The multi-instrumented studies of equatorial thermosphere aeronomy scintillation system: Climatology of zonal drifts, *J. Geophys. Res.*, *101*, 26,839–26,850.

Y. Chen, Center for Space Science and Applied Research, Chinese Academy of Sciences, 1 Nanertiao, Zhongguancun, Haidan District, Beijing 100012, China.

C. Ha Duyen and T. Le Truong, Hanoi Institute of Geophysics, Vietnamese Academy of Science and Technology, 18 Hoang Quoc Viet, Hanoi, Vietnam.

M. Ishii, M. Kubota, and T. Maruyama, National Institute of Information and Communications Technology, 4-2-1 Nukui-kita, Koganei, Tokyo 184-8795, Japan.

J. Li and G. Ma, National Astronomical Observatories, Chinese Academy of Sciences, 20A Datun Road, Chaoyang District, Beijing 100012, China.

S. Saito, Electronic Navigation Research Institute, 7-42-23 Jindaiji-Higashi, Chofu, Tokyo 182-0012, Japan. (susaito@enri.go.jp)

ATTACHMENT 3

ENRI'S LOCAL-AREA IONOSPHERE OBSERVATION SYSTEM IN ISHIGAKI, JAPAN

1. Location

The ENRI's local-scale ionosphere observation system is located on Ishigaki Island (24.3ºN, 124.2ºE) in the southwest part of Japan. Magnetic latitude of Ishigaki is about 19º. So it is usually on the poleward slope of EIA.

2. Observation sites

There are four sites in Ishigaki, separated by from 400 m to 1 km. The four sites include elementary Ishigaki and Heishin elementary schools, Ishigaki-2 junior-high school, and Ishigaki Athletic Park (Figure A3.1).

3. System description

At each site, a dual frequency (L1 and L2) GPS receiver (NovAtel Euro-3M) and a GPS scintillation receiver (GSV 4004B) are installed. Sampling rates are 2 and 50 Hz for gradient and scintillation measurements, respectively. Receivers share a dual frequency antenna (NovAtel GPS-702) mounted on top of the roof of a building. Some sites include more receivers and antennas for additional purposes. The system includes two factory PCs, one for gradient observation, and the other for scintillation. The PCs control receivers as well as receive data from the receivers. Data is recorded on hard disk drives. PCs are connected to ENRI via Internet, and can be controlled remotely (Figure A3.2).

4. Observation history

Scintillation observation has started from 2005, and gradient measurement from 2007.

Figure A3.1. Overview of the ENRI's local area ionosphere observation system in Ishigaki Island, Japan.

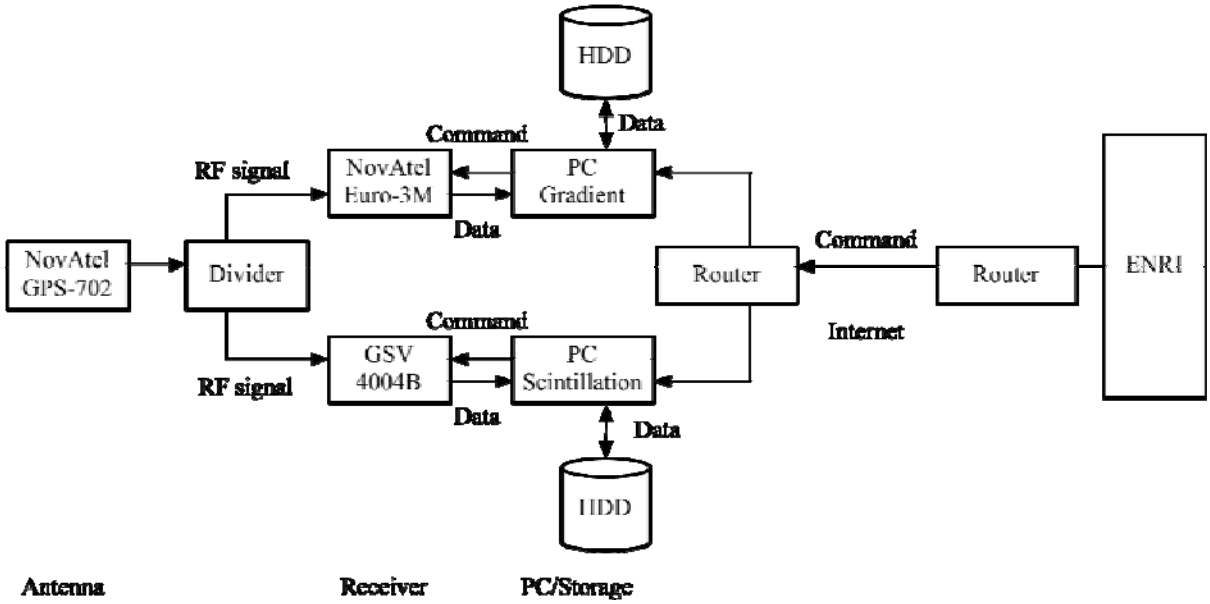

Figure A3.2. Simplified block diagram of the ENRI's local-area ionosphere observation system in Ishigaki Island.